의학석사 학위논문

2형 당뇨병 동물 모델에서 SGLT2 억제제의 신장 세포 노화 억제 효과

Effects of SGLT2 Inhibitor on Cellular Senescence in the Kidneys of Type 2 Diabetes Animal Model

2021년 2월

서울대학교 대학원
의학과 중개의학 전공

김 미 나

2형 당뇨병 동물 모델에서 SGLT2 억제제의 신장 세포 노화 억제 효과

Effects of SGLT2 Inhibitor on Cellular Senescence in the Kidneys of Type 2 Diabetes Animal Model

지도교수 조 영 민

이 논문을 의학 석사학위논문으로 제출함

2020 년 10 월

서울대학교 대학원

의학과 중개의학 전공

김 미 나

김미나의 석사학위논문을 인준함

2020 년 12 월

위 원 장 박 경 두 (인)

부 위 원 장 조 영 민 (인)

위 원 권 오 빈 (인)

Abstract

Effects of SGLT2 Inhibitor on Cellular Senescence in the Kidneys of Type 2 Diabetes Animal Model

Mi Na Kim

Major in Translational Medicine

College of Medicine

Seoul National University Graduate School

Introduction

Sodium-glucose cotransporter 2 (SGLT2) inhibitors prevent the progression of diabetic kidney disease. However, the mechanisms underlying this renoprotective benefit are not completely understood. I evaluated whether SGLT2 inhibition reduces cellular senescence in the kidney and investigated the molecular pathways involved in the renoprotective effect.

Methods

Dapagliflozin (1 mg/kg), glimepiride (2.5 mg/kg), or vehicle was administered daily via oral gavage for 8 weeks in *db/db* mice. Expression levels of aging marker genes (p21, p16, p53, γH2AX) were measured in the kidney using real-time RT-PCR, immunohistochemistry, and western blot analysis. For *in vitro* analysis, HK-2 cells, a human renal tubular epithelial cell line, were pretreated with H_2O_2 to induce cellular senescence, and the levels of aging markers were measured after treatment with β

-hydroxybutyrate (β-HB) or *NRF2*-specific siRNA.

Results

Mesangial expansion was ameliorated in the dapagliflozin-treated *db/db* (*db/db*+SGLT2i) group. Besides, in the *db/db*+SGLT2i group, the size of the glomerulus was smaller, and albuminuria was markedly reduced compared with the vehicle-treated *db/db* (*db/db*+vehicle) group. Expression levels of aging marker genes (p21, p16, p53, γH2AX) in the kidney were increased in the *db/db*+vehicle group compared with the *db*/+ group, and this increase was markedly reversed in the *db/db*+SGLT2i group, but not in the glimepiride-treated *db/db* (*db/db*+SU) group. In the kidneys of mice in the *db/db*+SGLT2i group, oxidative stress was also reduced compared with those in the *db/db*+vehicle and *db/db*+SU groups. Dapagliflozin increased plasma β-HB, which reduced H_2O_2-induced DNA damage and senescence in HK-2 cells. β-HB-induced NRF2 nuclear translocation mediated anti-senescent effects by inducing antioxidant pathways.

Conclusion

Dapagliflozin, an SGLT2 inhibitor, prevented the progression of diabetic kidney disease by inhibiting cellular senescence and oxidative stress in the kidneys via ketone-induced NRF2 activation.

Keywords : SGLT2 Inhibitor, Cellular Senescence, Diabetic Kidney Disease, Ketone Body, NRF2

Student Number : 2019-27807

Contents

Abstract (외국어 초록) ····· **i**
Contents ····· **iii**
List of tables and figures ····· **iv**
Introduction ····· **1**
Material and Methods ····· **4**
Results ····· **11**
Discussion ····· **38**
Acknowledgements ····· **42**
References ····· **43**
국문초록 ····· **48**

List of tables and figures

Table 1. Sequences of primers for real-time RT-PCR ····· 8

Figure 1. Schematic of the study design, body weight, blood glucose, and cumulative food intake during treatment ····· 11
Figure 2. Oral glucose tolerance test and plasma insulin levels ····· 12
Figure 3. Relative mRNA expression of *p21*, *p16*, and *p53* in the kidney ····· 14
Figure 4. Western blot and band intensities for p21, p16, p53BP1, and γH2AX of the kidney ····· 15
Figure 5. Representative blots of cytokine array of the kidney ····· 16
Figure 6. Representative images of PAS-stained sections of the kidney ····· 18
Figure 7. Urinary albumin to creatinine concentration ratio ····· 19
Figure 8. Representative images of SA β-gal staining of the kidney sections ·· 20
Figure 9. Immunofluorescence staining of γH2AX of the kidney sections ····· 21
Figure 10. Representative images of DHE-stained sections of the kidney ····· 22
Figure 11. Comparison of SOD activities in the kidney ····· 23
Figure 12. Plasma β-hydroxybutyrate concentrations ····· 25
Figure 13. Relative mRNA expression of *p21*, *p16*, and *p53* in HK-2 cells ··· 26
Figure 14. Representative images of SA β-gal staining in HK-2 cells ····· 27
Figure 15. Western blot and band intensity for p21, p16, p53BP1, and γH2AX of HK-2 cells ····· 28
Figure 16. Immunofluorescence staining of γH2AX in HK-2 cells ····· 29
Figure 17. Western blot for NRF2 in the kidney ····· 31
Figure 18. Immunofluorescence staining of NRF2 in HK-2 cells ····· 32
Figure 19. Protein levels of NRF2 in the cytoplasm, nucleus, and total lysates of HK-2 cells ····· 33

Figure 20. Relative mRNA expression of *NRF2*, *NQO1*, and *HO-1* in HK-2 cells ····· 34
Figure 21. Relative mRNA expression of *NRF2* in siNC- or si*NRF2*-transfected HK-2 cells and relative mRNA expression of *p21*, *p16*, and *p53* with or without β-HB in siNC- or si*NRF2*-transfected HK-2 cells ····· 35
Figure 22. Protein expression of p21, p16, p53BP1, and γH2AX with or without β-HB in siNC- or si*NRF2*-transfected HK-2 cells ····· 36

Introduction

Diabetic kidney disease (DKD), a major microvascular complication of diabetes, is the leading cause of end-stage renal disease (ESRD) globally [1]. The main pathological features of DKD include thickening of the glomerular basement membrane, mesangial expansion, and podocyte damage [2]. Hemodynamic changes including glomerular hyperfiltration and an increase in intraglomerular pressure promote the progression of DKD [3]. In the diabetic kidney, increased renal filtration of glucose results in increased reabsorption of sodium and glucose via the sodium-glucose cotransporters, SGLT1 and 2, which are located in the brush border membrane in S3 and S1 segments of the proximal tubule, respectively [4]. Consequently, a lesser amount of sodium reaches the macula densa, resulting in reduced tubuloglomerular feedback via the juxtaglomerular apparatus. This leads to the dilation of the renal afferent arterioles, inducing glomerular hyperfiltration, which leads to further renal damage [5]. Under these conditions, SGLT2 inhibition drastically reduces sodium and glucose reabsorption in the proximal tubule, which in turn recovers an adequate amount of sodium reaching the macula densa. Therefore, normal tubuloglomerular feedback is resumed, which prevents further kidney damage by lowering the intraglomerular pressure [6-8].

In addition to the renal hemodynamic effect, SGLT2 inhibitors also mitigate renal hypoxia and create a negative energy balance, which are both potential renoprotective mechanism. Hypoxia has been suggested as a common pathway for DKD and ESRD [9, 10]. In the kidneys, most of the oxygen is utilized for tubular sodium reabsorption through the action of Na^+/K^+-ATPase [11], which could be reduced by SGLT2 inhibition. SGLT2 inhibition reduced oxidative stress via induction of hypoxia-inducible factor 1 in the kidneys of diabetic mice [12, 13].

The kidneys with DKD were shown to undergo accelerated cellular senescence in renal cells, mainly tubule cells, in the human diabetic kidney because hyperglycemic stress triggers the elevation of senescence associated β-galactosidase (SA β-gal) and cell cycle inhibitor p16 [14]. Accumulation of these senescent cells may induce age-related

dysfunction [15]. Therefore, reducing cellular senescence is important for the development of type 2 diabetes and its complications. In this regard, SGLT2 inhibitors could be a viable option to tackle this issue as discussed below.

Renal glucose reabsorption requires energy to overcome glucose concentration gradient across the tubular cell membrane. SGLT2 is responsible up to 90% of glucose reabsorption from the proximal tubule. To reabsorb glucose against the concentration gradient, SGLT2 uses the sodium ion gradient which is generated by the action of Na^+/K^+-pump on the basolateral membrane, which requires ATP synthesized by oxidative phosphorylation [16]. Indeed, 80% of oxygen consumption in the kidney is related to the generation of the sodium ion gradient [17]. As a by-product of oxidative phosphorylation, reactive oxygen species (ROS) is inevitably produced, which leads to cellular damage and senescence [18]. On the other hand, SGLT2 inhibition leads to a negative energy balance due to its glycosuric effect, and therefore, SGLT2 inhibitors are potential calorie restriction mimetics [19]. Either calorie restriction or canagliflozin, an SGLT2 inhibitor, increased the life span and delayed the onset of age-related disorders in animal studies [20-22]. Intriguingly, both SGLT2 inhibitor and calorie restriction increase the plasma concentrations of ketone bodies [23], which may share common mechanisms to relieve age-related disorders. Therefore, SGLT2 inhibition may reduce oxidative stress by blocking the Na^+/K^+-ATPase and inducing a negative energy balance, suggesting anti-senescent effects in the kidney.

SGLT2 inhibitors reduce cardiovascular events, particularly the risk of hospitalization for heart failure in type 2 diabetes patients with cardiovascular disease or multiple cardiovascular risk factors [7, 8, 24]. Besides, SGLT2 inhibitors also decrease renal outcomes, including a sustained decrease in the estimated glomerular filtration rate (eGFR), progression to ESRD, or death from renal or cardiovascular causes in patients with type 2 diabetes [7, 25, 26]. Interestingly, the renoprotective effect of SGLT2 inhibitors was independent of its glucose-lowering effect [5]. Indeed, in the DAPA-CKD study, dapagliflozin reduced the risk of worsening kidney function or death from cardiovascular disease in patients with chronic kidney disease, even without type 2 diabetes [27].

In this study, I examined the effect of SGLT2 inhibition using dapagliflozin on DKD in *db/db* mice, a type 2 diabetes animal model shown to the phenotypes including glomerulus hypertrophy and albuminuria [28], primarily focusing on cellular senescence and oxidative stress.

Materials and Methods

Animals

Six-week-old male *db/db* mice and lean *db*/+ mice were obtained from Japan SLC (Shizuoka, Japan). All animals had access to a chow diet and water *ad libitum*. At 15 weeks of age, the mice were divided into four groups: (1) *db*/+ (as normal control), (2) *db/db*+vehicle (drinking water), (3) *db/db*+SGLT2i (dapagliflozin, 1 mg/kg), and (4) *db/db*+SU (glimepiride, 2.5 mg/kg). Dapagliflozin (11574, Cayman Chemicals, Ann Arbor, MI, USA), glimepiride (12090, Cayman Chemicals) or vehicle was administered daily via oral gavage for 8 weeks. Body weight, blood glucose, and daily food intake were measured twice a week during the treatment. After 8 weeks, all animals were anesthetized using 2% isoflurane inhalation, tissues were rapidly obtained, and euthanized. This study was approved by the Animal Care and Use Committee at Seoul National University Hospital (approved number: 19-0072-S1A0).

Oral glucose tolerance test

After 7 weeks of treatment, the oral glucose tolerance test (OGTT) was performed after overnight fasting (~16 h). Fasted mice were weighed and orally administered 20% glucose solution (1 g/kg body weight). Glucose levels were measured in blood drawn from the tail vein at 0, 15, 30, 60, and 120 min using a glucometer (Accu-chek, Roche Diagnostics, Mannheim, Germany). For plasma insulin measurement, blood from the tail vein was collected in heparinized microhematocrit tubes, and plasma was separated via centrifugation at 1500 g for 10 min and 4°C. Plasma insulin levels were measured using a Mouse Insulin ELISA Kit (90080, Crystal Chem, Downers Grove, IL, USA) according to the manufacturer's instructions.

Biochemical analysis

Urine samples were collected from the mice housed in metabolic cages. Urine albumin and creatinine concentrations were measured using a Mouse Albumin ELISA

Kit and a Mouse Creatinine Kit (80630, 80350, Crystal Chem, respectively). Plasma β-HB (700190, Cayman Chemicals) and superoxide dismutase (SOD) activity (ab65354, Abcam, Cambridge, MA, USA) were assessed using commercial colorimetric assay kits.

Cell culture

A human renal tubular epithelial cell line (HK-2) were purchased from the Korean Cell Line Bank for *in vitro* experiments. HK-2 cells were cultured in RPMI 1640 supplemented with 10% fetal bovine serum (Hyclone, Logan, UT, USA) and 1% penicillin and streptomycin in a 5% CO_2 incubator at 37°C. HK-2 cells were incubated with or without β-HB (3 mmol/L; GK-7020, Glentham Life Sciences, Wimbledon, London, UK) for 24 h, followed by H_2O_2 (500 μmol/L; H325-500, Fisher Scientific, Waltham, USA) treatment for 6 h.

siRNA transfection

HK-2 cells were seeded at a density of 5×10^5 cells per well in a 6-well plate and cultured for 24 h. Cells were then transfected with 50 nM *NRF2* small interfering (si) RNA (si*NRF2*; s9493, Thermo Fisher Scientific, Waltham, MA, USA) or negative control siRNA (siNC; AM4611, Thermo Fisher Scientific) using Lipofectamine RNAiMAX Transfection Reagent (13778, Invitrogen, Carlsbad, CA, USA) according to the manufacturer's instruction. After 24 h of transfection, the cells were stimulated with H_2O_2 in the presence or absence of β-HB, and samples were harvested for further RNA or protein analysis.

SA β-galactosidase assay

Senescent cells of kidney tissues and HK-2 cells were evaluated with a SA β-gal staining kit (9860, Cell Signaling Technology, Danvers, MA, USA). For comparing senescent cells in each group, frozen tissues were embedded in optimal cutting temperature (OCT) compound (Tissue-Tek OCT, Ted Pella Inc., CA, USA) and cut with a cryostat, and cells were seeded in a 6-well plate. Subsequently, slides and cells were

incubated with fixatives for 10 min at room temperature (RT), washed with phosphate-buffered saline (PBS), and incubated with β-galactosidase staining solution (pH 6.0) at 37°C overnight in a dry incubator. After washing, the slides were counterstained with eosin. Finally, senescent cells were evaluated under a Nikon Eclipse Ci-L microscope with a ×400 magnification (Nikon Corporation, Tokyo, Japan).

Histology and immunofluorescence staining

Mouse kidney tissues were harvested and fixed in 4% paraformaldehyde at 4°C overnight. The tissues were paraffin-embedded, and sections were cut at a thickness of 4 μm. Slides were either stained with periodic acid–Schiff's (PAS) reagent to evaluate mesangial expansion or deparaffinized in xylene and then washed with serial ethanol diluent for immunofluorescence staining. Dewaxed sections were subjected to antigen retrieval using Target Retrieval Solution (S1700, Dako North America, Carpinteria, CA, USA). Sections were then blocked with 5% goat serum in antibody diluent (S2022, Dako North America) for 1 h at RT and incubated overnight at 4°C with rabbit anti-γH2AX antibody (1:100, 9718, Cell Signaling). After rinsing with Tris-buffered saline containing 0.05% Tween 20, sections were incubated with Alexa Fluor 488 goat anti-rabbit secondary antibody (1:200, A27034, Invitrogen) for 1 h at RT and mounted with DAPI (H-1500, Vector Laboratories, Burlingame, CA, USA). Images were acquired under a confocal microscope (Leica TCS STED CW, Leica Microsystems, Wetzlar, Germany) and analysed using MetaMorph Image Analysis (Molecular Devices, San Jose, CA, USA).

Immunocytochemistry

HK-2 cells were plated at a density of 3×10^5 cells per well on cell culture slides (30104, SPL Life Sciences, Gyeonggi-do, Korea) coated with poly-d-lysine (Sigma-Aldrich, St Louis, MO, USA) to enhance cell attachment. The cells were incubated with or without β-HB, followed by H_2O_2 stimulation. After treatment, the cells were washed with PBS and fixed in 4% paraformaldehyde for 15 min. The fixed cells were blocked with 5% goat serum and incubated with the corresponding primary

antibody (1:100) overnight at 4°C. Next, the cells were incubated with Alexa Fluor 488 goat anti-rabbit secondary antibody (1:200) for 2 h and counterstained with DAPI. Finally, images were obtained under a confocal microscope (Leica).

Measurement of ROS

ROS levels were determined using dihydroethidium (DHE) staining. Cryosection was performed in OCT compound-embedded frozen tissues and HK-2 cells were seeded in a glass slide for further staining. Frozen kidney sections and HK-2 cells were incubated with DHE (5 μmol/L; Sigma-Aldrich) solution in a humidified chamber at 37°C for 30 min and then counterstained with DAPI. Fluorescence intensity (excitation at 535 nm, emission at 610 nm) was measured using a confocal microscope (Leica).

Real-time RT-PCR

Total RNA was extracted from tissue samples and HK-2 cells using a Total RNA Extraction Kit (Intron, Seoul, Korea) and 1 μg of RNA was reverse transcribed using a reverse transcription kit (Promega, Madison, Wisconsin, USA). Real-time RT-PCR was performed with a SYBR Green Master Mix (Takara, Otsu, Shiga, Japan) using an ABI 7500 real-time PCR system (Applied Biosystems, Foster City, CA, USA) to evaluate the mRNA expression of *p21*, *p16*, *p53*, *NRF2*, *NQO1*, and *HO-1*. 18S rRNA (mouse) and *GAPDH* (human) were used as internal controls. The sequences of the primers are shown in Table 1.

Table 1. Sequences of primers for real-time RT-PCR

Gene	Forward primer sequences	Reverse primer sequences
p21 (M)	GGTTCCTTGCCACTTCTT	GAGTCGGGATATTACGGTTG
p16 (M)	TTGGCCCAAGAGCGGGGACA	GCGGGCTGAGGCCGGATTTA
p53 (M)	ACCGCCGACCTATCCTTACC	TCTTCTGTACGGCGGTCTCTC
18s (M)	AGTCCCTGCCCTTTGTACACA	GATCCGAGGGCCTCACTAAAC
p21 (H)	GAGGCCGGGATGAGTTGGGAGGAG	CAGCCGGCGTTTGGAGTGGTAGAA
p16 (H)	CCAACGCACCGAATAGTTACG	GCGCTGCCCATCATCATG
p53 (H)	CCCCTCCTGGCCCCTGTCATCTTC	GCAGCGCCTCACAACCTCCGTCAT
NRF2 (H)	CACATCCAGTCAGAAACCAGTGG	GGAATGTCTGCGCCAAAAGCTG
NQO1 (H)	CCTGCCATTCTGAAAGGCTGGT	GTGGTGATGGAAAGCACTGCCT
HO-1 (H)	CCAGGCAGAGAATGCTGAGTTC	AAGACTGGGCTCTCCTTGTTGC
GAPDH (H)	AGGGCTGCTTTTAACTCTGGT	CCCCACTTGATTTTGGAGGGA

Abbreviation : M; mouse, H; human

Western blot analysis

Total protein was extracted from tissue samples and HK-2 cells using RIPA buffer containing a protease/phosphatase inhibitor. Separation of cytoplasmic and nuclear extracts was performed using the NE-PER Nuclear and Cytoplasmic Extraction Reagents Kit (Thermo Fisher Scientific). Lysates were centrifuged at 16,000 g for 15 min, and the supernatants were boiled for 5 min at 100°C. Samples with equal amounts of the protein were separated via electrophoresis in 4–15% precast protein gels (456-1084, Bio-Rad, Hercules, CA, USA) and then transferred onto a polyvinylidene difluoride membrane. The membranes were blocked in 5% skim milk for 1 h and incubated overnight at 4°C with the following primary antibodies: anti-p53BP1 (1:1000, A300-272A, Bethyl Laboratories, Montgomery, TX, USA), anti-p21 (1:1000, 556430, BD Biosciences, San Jose, CA, USA), anti-p16 (1:1000, ab211542, Abcam), anti-γH2AX (1:1000, 9718, Cell Signaling), anti-NRF2 (1:1000, 12721, Cell Signaling), anti-LAMIN B1 (1:1000, 12586, Cell Signaling), and anti-GAPDH (1:1000, 5174, Cell Signaling). Blots were incubated with respective HRP-conjugated secondary antibodies (1:5000) for 1 h at RT, visualized using a chemiluminescent substrate (Thermo Fisher Scientific), and captured using an Amersham Imager 680 (GE Healthcare, Chicago, IL, USA). The captured images were quantified using Image J software (NIH, Bethesda, MD, USA) and normalized to the expression levels of GAPDH.

Cytokine array

Cytokine arrays (AAM-CYT-3-2, Mouse Cytokine Array C3, RayBiotech, Norcross, GA, USA) were performed according to the manufacturer's instructions. In brief, proteins were extracted from kidney tissues using RIPA buffer containing a protease/phosphatase inhibitor cocktail. After blocking, the membranes were incubated with 1 ml of diluted sample (250 μg of tissue extract in 1× blocking buffer) at 4°C overnight. The membranes were washed with wash buffer and incubated with a biotinylated antibody cocktail followed by diluted HRP-conjugated streptavidin. After washing, the membranes were incubated in detection buffer and imaged with an

Amersham Imager 680. Each spot of the captured images was quantified using Image J.

Statistical analysis

All data were expressed as the mean ± standard error of the mean (SEM). Statistical analyses between groups were performed using Student's *t* test or ANOVA multiple comparisons with Tukey's post-hoc test using GraphPad Prism 7 (GraphPad Software, La Jolla, CA, USA). A *P* value of <0.05 was considered statistically significant.

Results

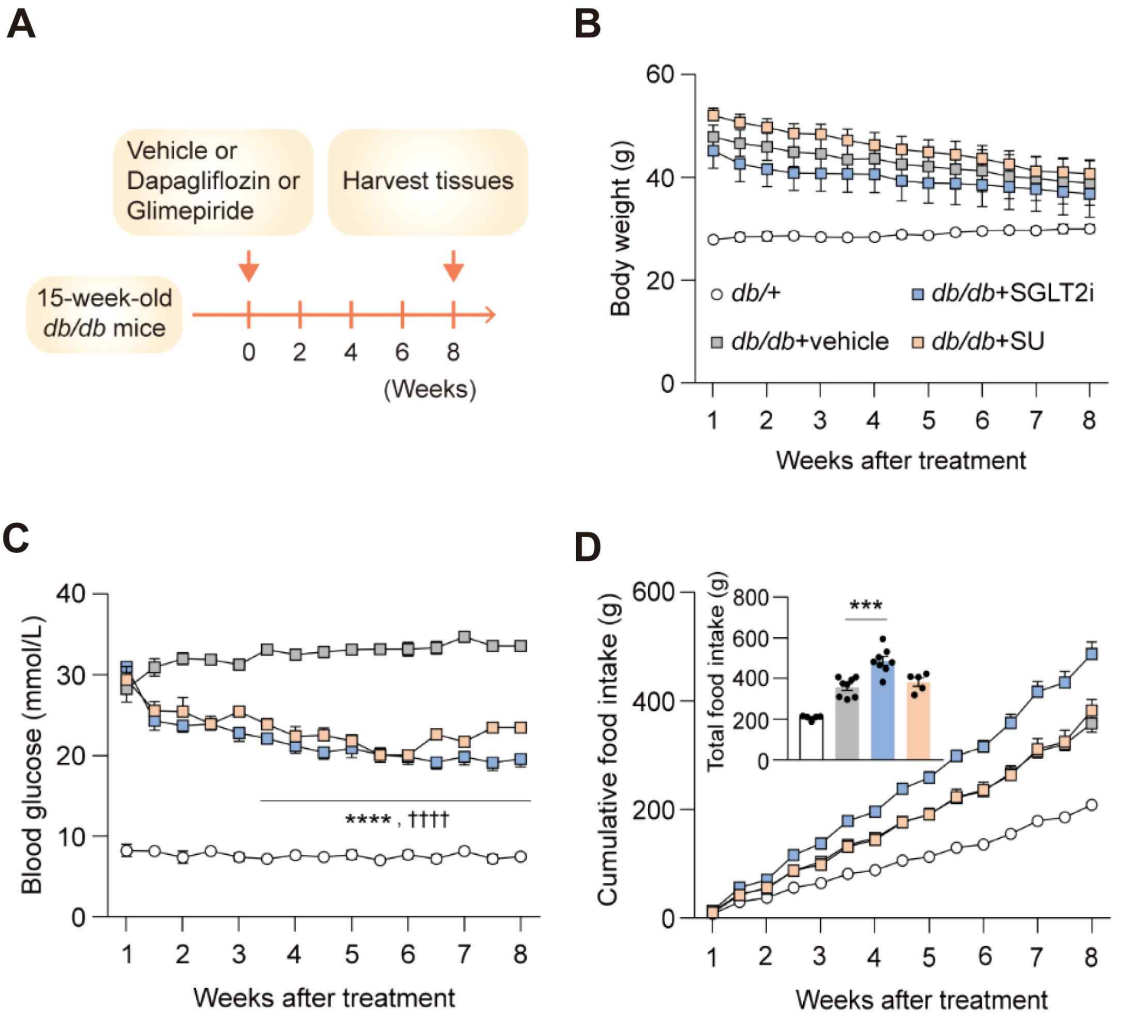

Figure 1. Schematic of the study design, body weight, blood glucose, and cumulative food intake during treatment

(A) Schematic of the study design. Vehicle, dapagliflozin (1 mg/kg/day), and glimepiride (2.5 mg/kg/day) were administered to 15-week-old *db/db* mice. (B) Body weight, (C) blood glucose, and (D) cumulative food intake of mice in *db*/+ (n = 5), *db/db*+vehicle (n = 8), *db/db*+SGLT2i (n = 8), *db/db*+SU (n = 5) groups for 8 weeks. ***p < 0.001, ****p < 0.0001 for *db/db*+SGLT2i vs *db/db*+vehicle; $^{††††}p$ < 0.0001 for *db/db*+SU vs *db/db*+vehicle

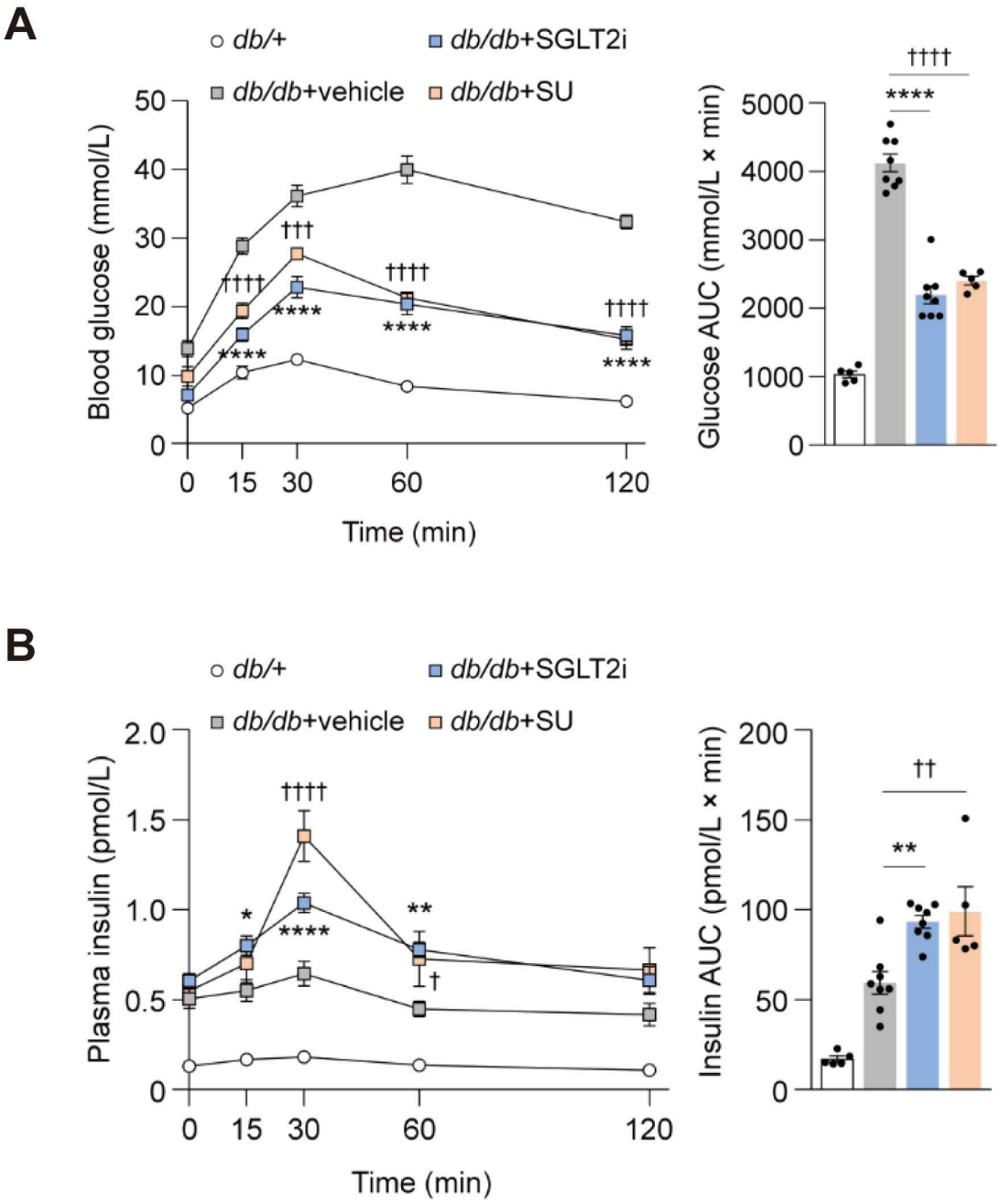

Figure 2. Oral glucose tolerance test and plasma insulin levels

(A) Blood glucose concentrations and the corresponding AUC, (B) plasma insulin levels and the corresponding AUC during the oral glucose tolerance test after 7 weeks of treatment (n = 5–8 per group). *p < 0.05, **p < 0.01, ***p < 0.001, and ****p < 0.0001 for *db/db*+SGLT2i vs *db/db*+vehicle; $^{\dagger}p < 0.05$, $^{\dagger\dagger}p < 0.01$, $^{\dagger\dagger\dagger}p < 0.001$, and $^{\dagger\dagger\dagger\dagger}p < 0.0001$ for *db/db*+SU vs *db/db*+vehicle

Dapagliflozin improves glucose homeostasis in *db/db* mice

To evaluate the metabolic effects of dapagliflozin, an SGLT2 inhibitor, 15-week-old *db/db* mice were treated with vehicle (*db/db*+vehicle), glimepiride (*db/db*+SU), or dapagliflozin (*db/db*+SGLT2i) for 8 weeks (Fig. 1A). Body weights were comparable among the three groups, with the *db/db*+SGLT2i group exhibiting nominally the lowest values (Fig. 1B). Blood glucose levels were comparable between the *db/db*+SU and *db/db*+SGLT2i groups. However, both these groups had significantly lower blood glucose levels compared with the *db/db*+vehicle group (Fig. 1C). Total food intake was similarly increased in the *db/db*+vehicle and *db/db*+SU groups compared with the *db*/+ group. Interestingly, the *db/db*+SGLT2i group showed significantly higher food intake compared with the *db/db*+vehicle and *db/db*+SU groups (Fig. 1D). During the OGTT performed after 7 weeks of treatment, blood glucose levels of the *db/db*+SU and *db/db*+SGLT2i groups were significantly lower than those of the *db/db*+vehicle group (Fig. 2A). Insulin secretion during the OGTT was improved in the *db/db*+SU and *db/db*+SGLT2i groups (Fig. 2B).

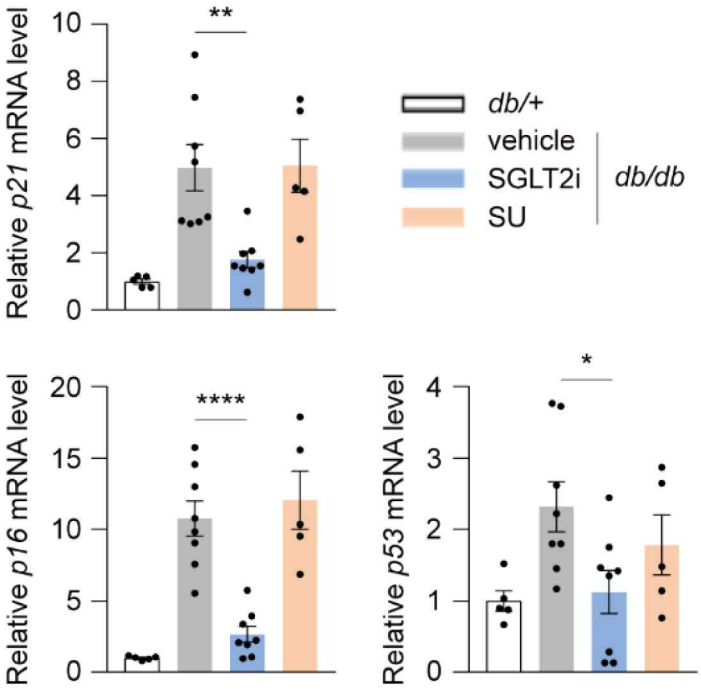

Figure 3. Relative mRNA expression of *p21*, *p16*, and *p53* in the kidney

Relative mRNA expression of *p21*, *p16*, and *p53* in the kidney. The value was normalized against 18S expression (n = 5–8 per group). *p < 0.05, **p < 0.01, and ****p < 0.0001 vs *db/db*+vehicle

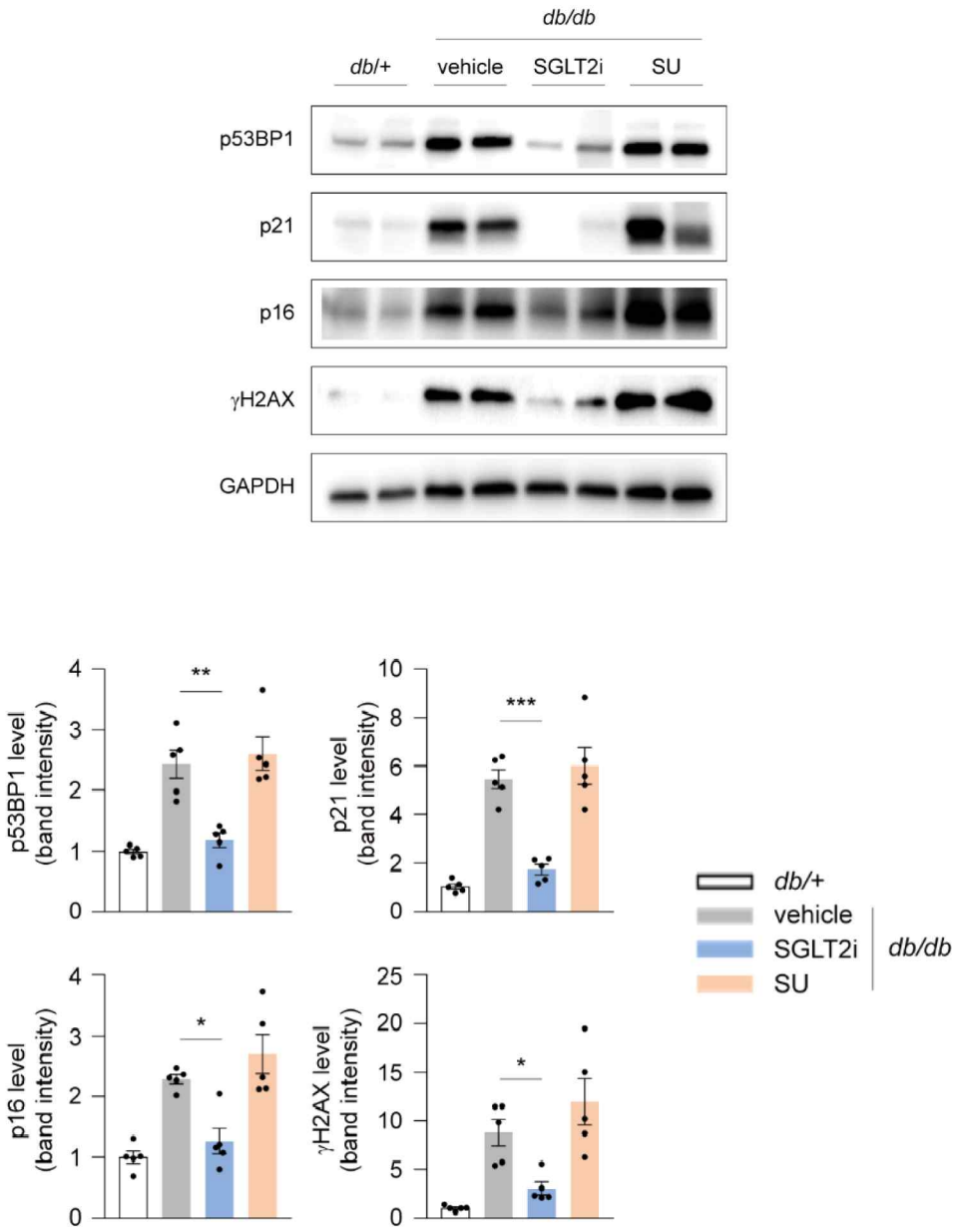

Figure 4. Western blot and band intensities for p21, p16, p53BP1, and γH2AX of the kidney

Western blot and band intensities for p21, p16, p53BP1, and γH2AX of the kidney (n = 5 per group). *p < 0.05, **p < 0.01, and ***p < 0.001 vs *db/db*+vehicle

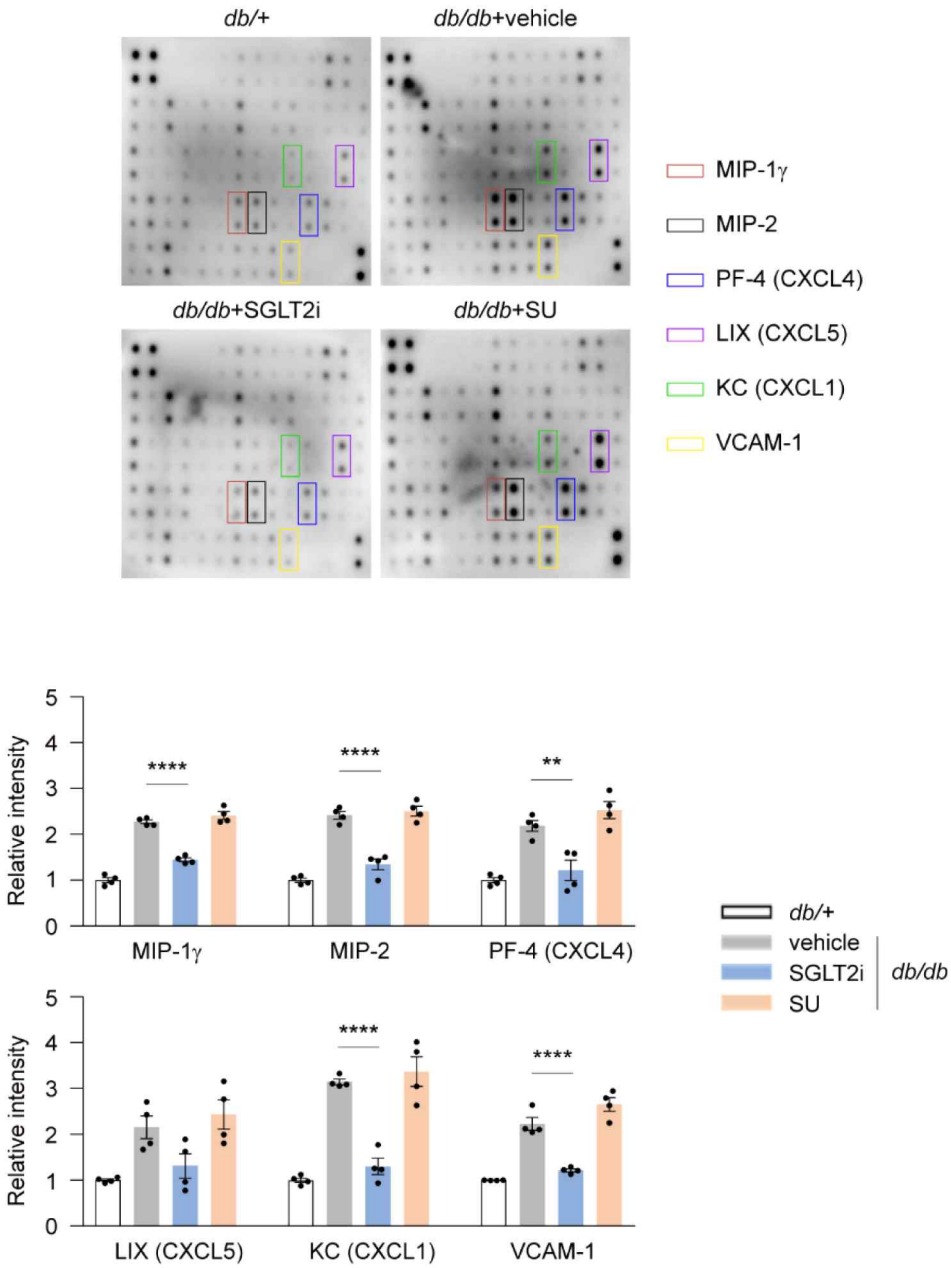

Figure 5. Representative blots of cytokine array of the kidney

Representative blots of cytokine array of the kidney and quantification of MIP-1γ, MIP-2, PF4, LIX, KC, and VCAM-1 (n = 4 per group). **p < 0.01, ****p < 0.0001 vs *db/db*+vehicle

Dapagliflozin reduces senescence and inflammation in the kidney of *db/db* mice

To evaluate the anti-senescent effects of dapagliflozin, I investigated the gene expression of the aging markers in the kidney. The mRNA levels of the aging markers, including *p21*, *p16* and *p53* in the kidney, were increased in the *db/db*+vehicle group compared with the *db*/+ group. However, this increase was markedly reversed in the *db/db*+SGLT2i group, but such improvement was not observed in the *db/db*+SU group, even though both groups showed similar glucose levels (Fig. 3). Protein expression of aging markers and DNA damage marker (γH2AX) were consistent with the mRNA levels (Fig. 4). Next, I examined the expression levels of senescence-associated secretory phenotype (SASP) in the kidney using a cytokine array. Interestingly, the levels of MIP-1γ, MIP-2, and CXCL-related cytokines were increased in the *db/db*+vehicle and *db/db*+SU groups but were significantly downregulated in the *db/db*+SGLT2i group (Fig. 5). These results suggest that dapagliflozin has anti-senescent and anti-inflammatory properties in the diabetic kidney, which is independent of its glucose-lowering effect.

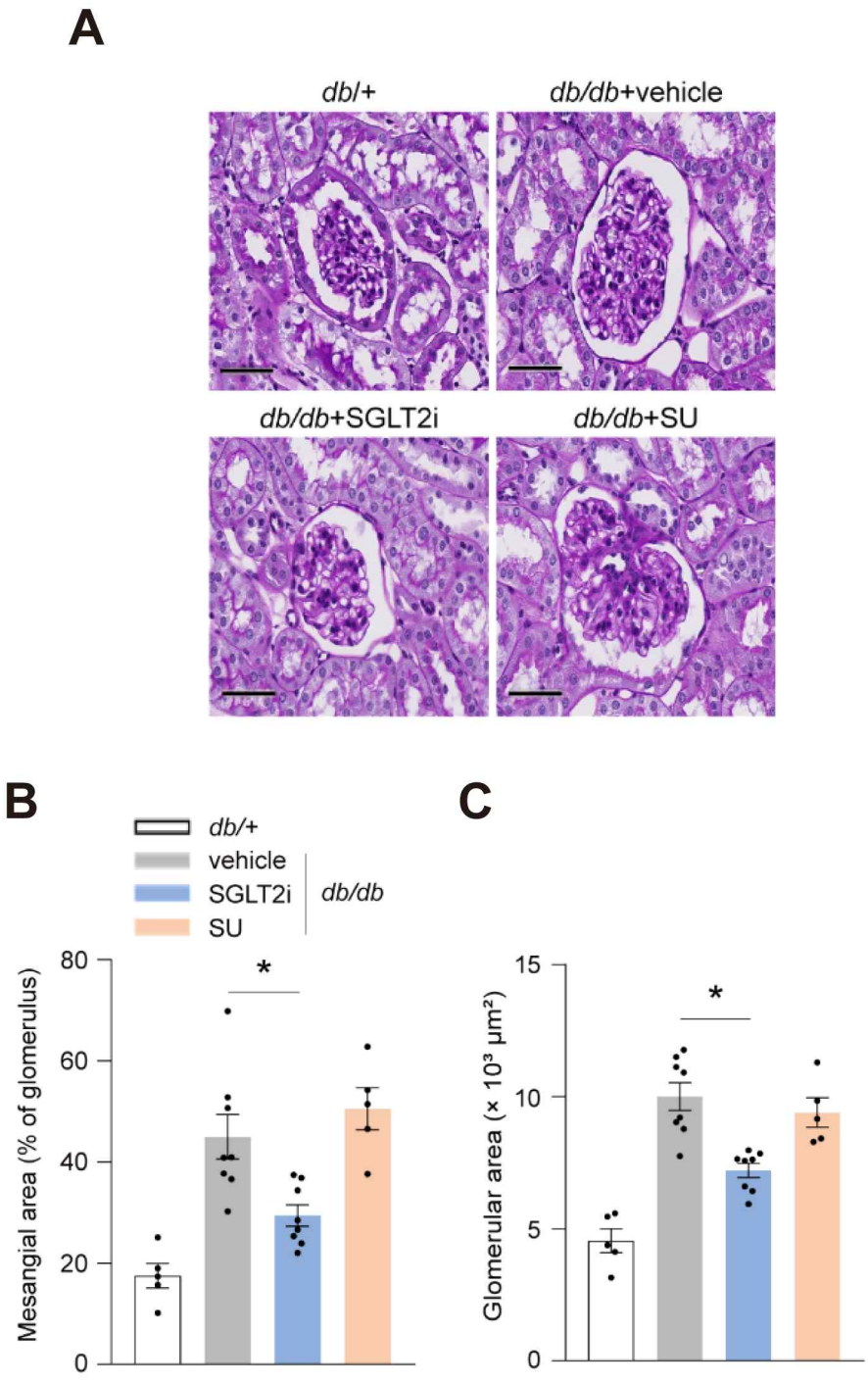

Figure 6. Representative images of PAS-stained sections of the kidney

(A) Representative images of PAS-stained sections of the kidney, (B) mesangial area, and (C) glomerular area (n = 5–8 per group). *P < 0.05 vs *db/db*+vehicle. Scale bars=50 μm.

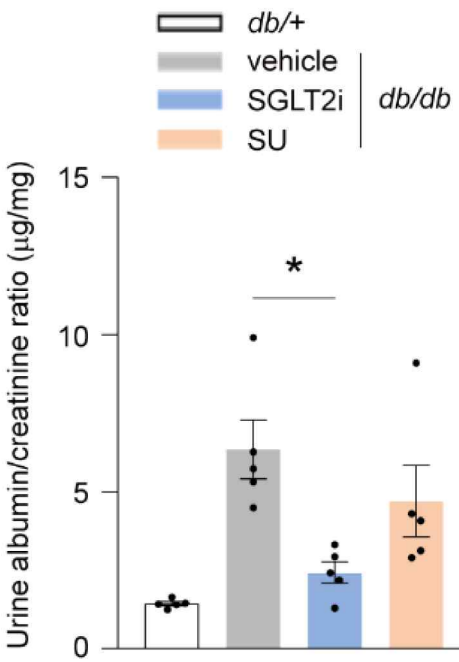

Figure 7. Urinary albumin to creatinine concentration ratio

Urinary albumin to creatinine concentration ratio (n = 5 each group). *P < 0.05 vs *db/db*+vehicle

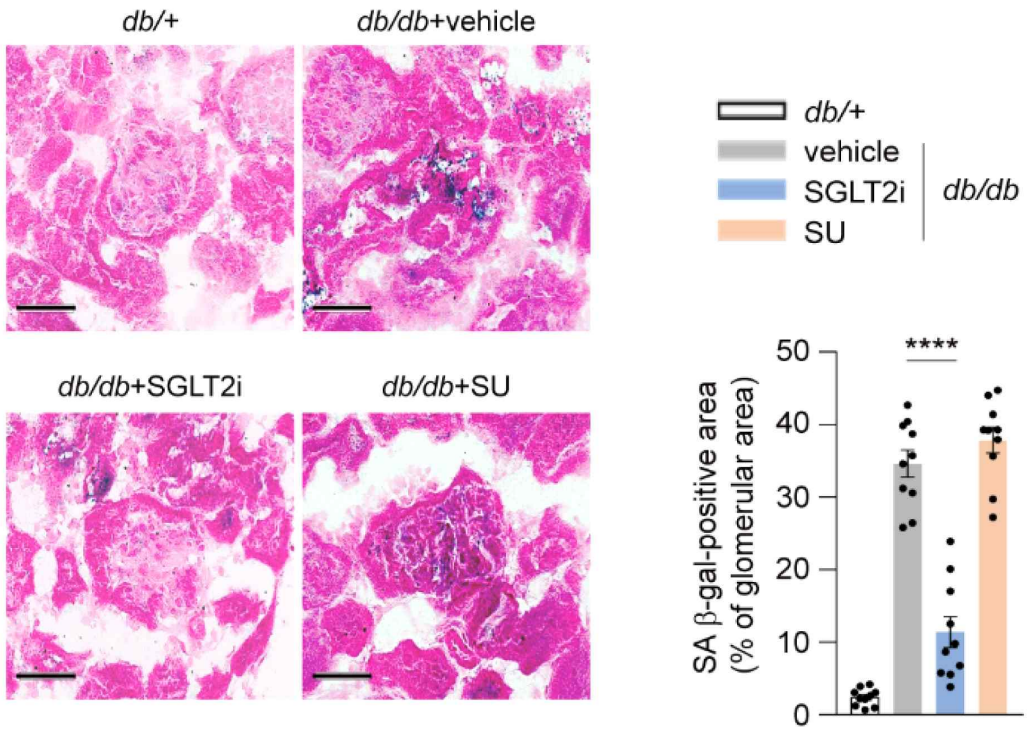

Figure 8. Representative images of SA β-gal staining of the kidney sections

Representative images of SA β-gal staining of frozen kidney sections and quantification of the SA β-gal positive area (n = 10 per group). ****p < 0.0001 vs *db/db*+vehicle. Scale bars=50 μm.

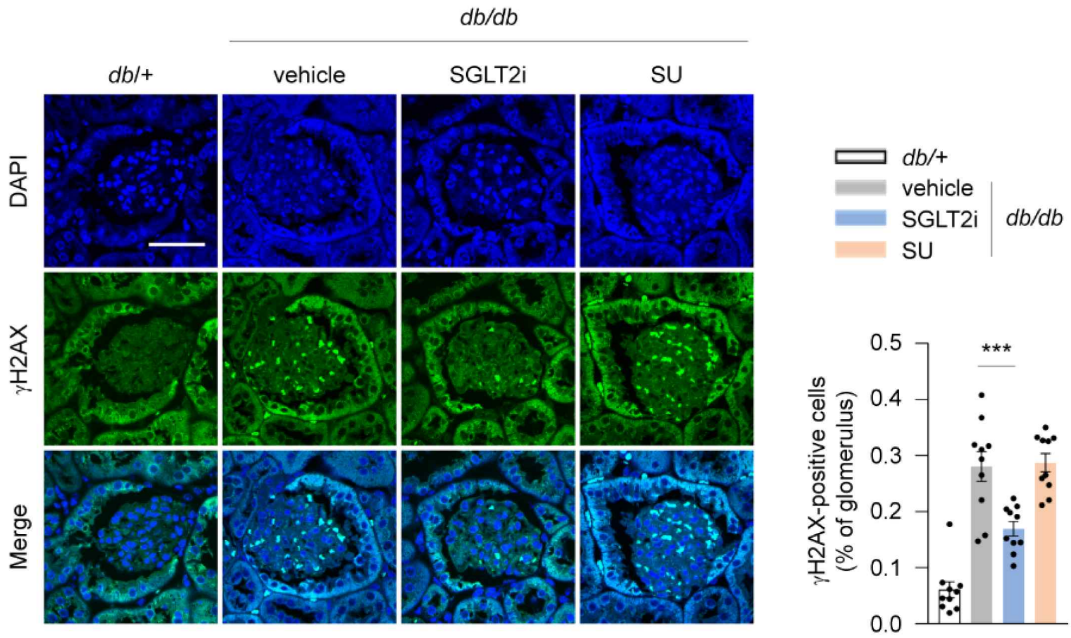

Figure 9. Immunofluorescence staining of γH2AX of the kidney sections

Immunofluorescence staining of γH2AX in the kidney sections and the number of γ H2AX-positive cells (% of glomerulus) counted for each group (n = 10 per group). ***p < 0.001 vs *db/db*+vehicle. Scale bars=50 μm.

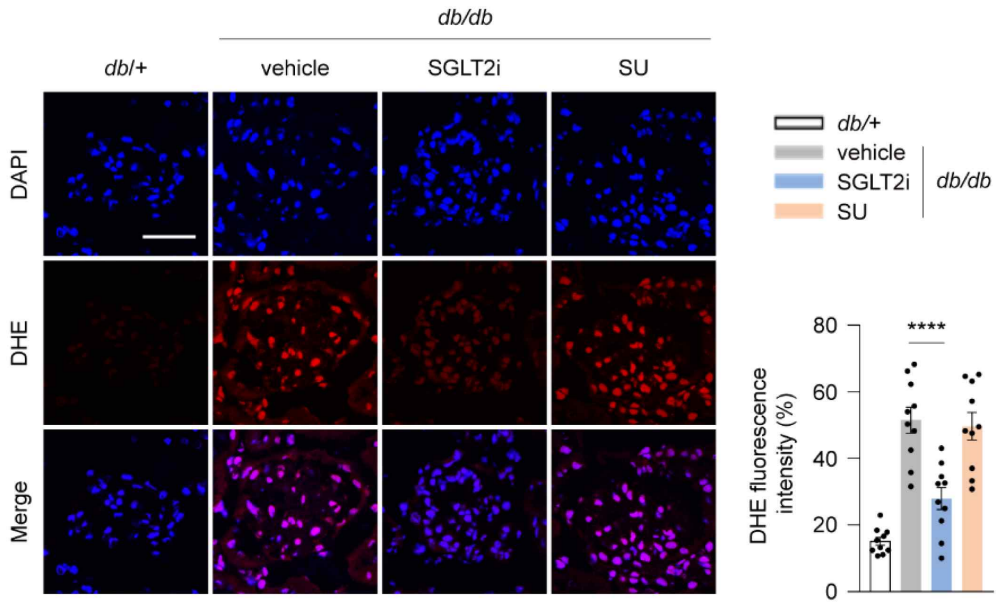

Figure 10. Representative images of DHE-stained sections of the kidney

Representative images of DHE-stained sections of the kidney and their intensities measured as an indicator of ROS level (n = 10 per group). ****p < 0.0001 vs *db/db*+vehicle. Scale bars=50 μm.

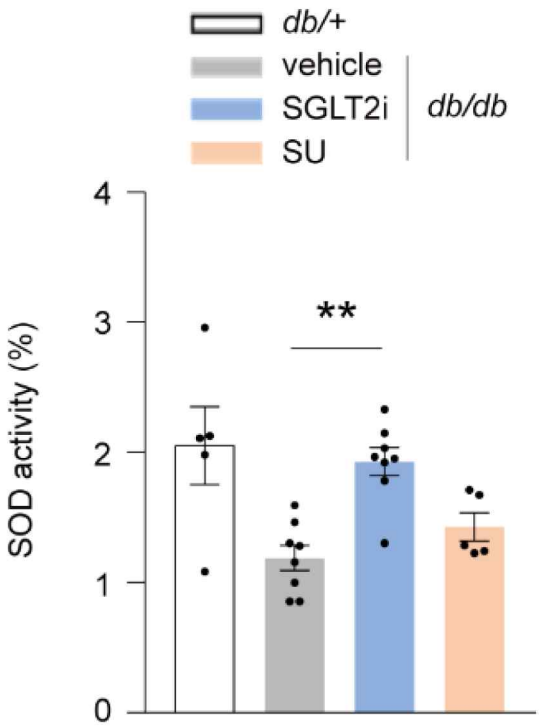

Figure 11. Comparison of SOD activities in the kidney

Comparison of SOD activities in the kidney (n = 5–8 per group). $^{**}P < 0.01$ vs *db/db*+vehicle

Dapagliflozin improves the phenotypes of diabetic kidney disease in *db/db* mice

I investigated whether the anti-senescent property of dapagliflozin improved the phenotypes of DKD. Mesangial expansion, a representative phenotype of DKD, was ameliorated in the *db/db*+SGLT2i group but not in the *db/db*+SU group (Fig. 6A). Besides, in the *db/db*+SGLT2i group, the size of glomerulus was smaller, and albuminuria was markedly reduced compared with the *db/db*+vehicle group (Fig. 6B, 7). The expression levels of SA β-gal and γH2AX were decreased in the glomerulus of the *db/db*+SGLT2i group, suggesting that SGLT2 inhibitors reduced senescence and DNA damage in the glomerulus of the SGLT2 inhibitor-treated kidney (Fig. 8, 9). Furthermore, glomeruli and tubules of the *db/db*+SGLT2i group showed lower levels of ROS compared with the *db/db*+vehicle and *db/db*+SU groups (Fig. 10). Similarly, antioxidant activity, measured by SOD activity, was higher in the *db/db*+SGLT2i group than in the *db/db*+vehicle group (Fig. 11). Given that senescence is known to increase oxidative stress and inhibit the activity of antioxidant enzymes [29-31], these results suggest that SGLT2 inhibition reduces cellular senescence by reducing ROS levels, possibly by activating the antioxidant system.

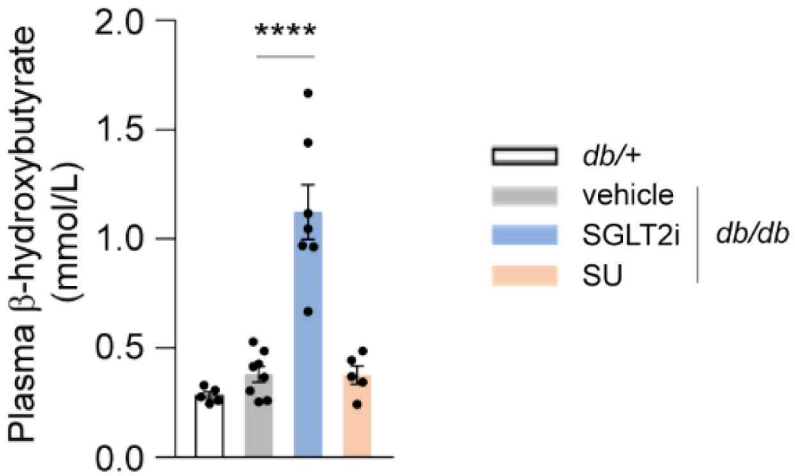

Figure 12. Plasma β-hydroxybutyrate concentrations

Plasma β-hydroxybutyrate concentrations (n = 5–8 per group). ****p < 0.0001 vs *db/db*+vehicle

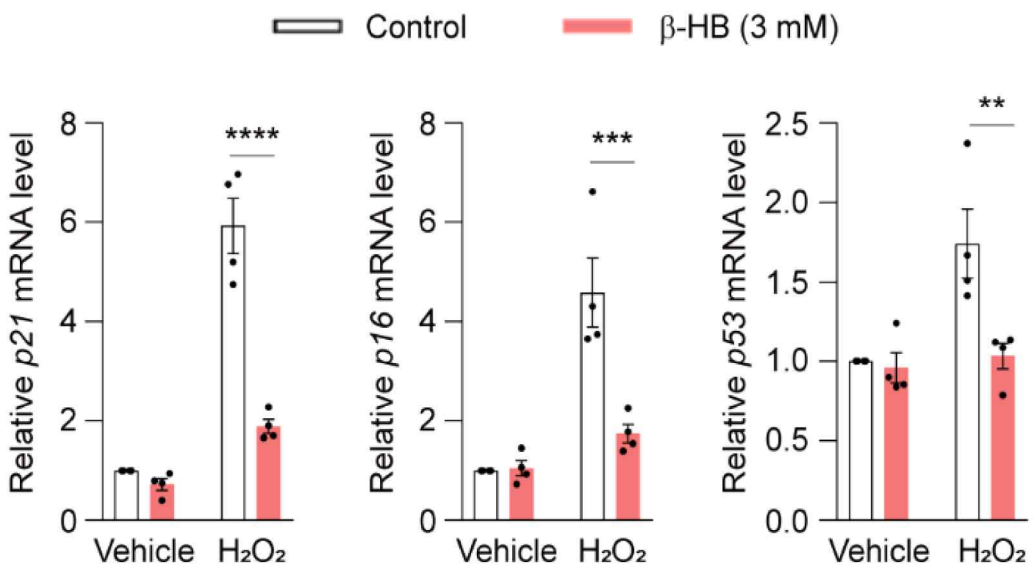

Figure 13. Relative mRNA expression of *p21*, *p16*, and *p53* in HK-2 cells

HK-2 cells were incubated with or without β-HB (3 mmol/L) for 24 h before H_2O_2 (500 μmol/L) stimulation for 6 h. Relative mRNA expression of *p21*, *p16*, and *p53* in the treated HK-2 cells. The value was normalized against *GAPDH* expression (n = 4 per group). $^{**}p < 0.01$, $^{***}p < 0.001$, and $^{****}p < 0.0001$ vs H_2O_2 only

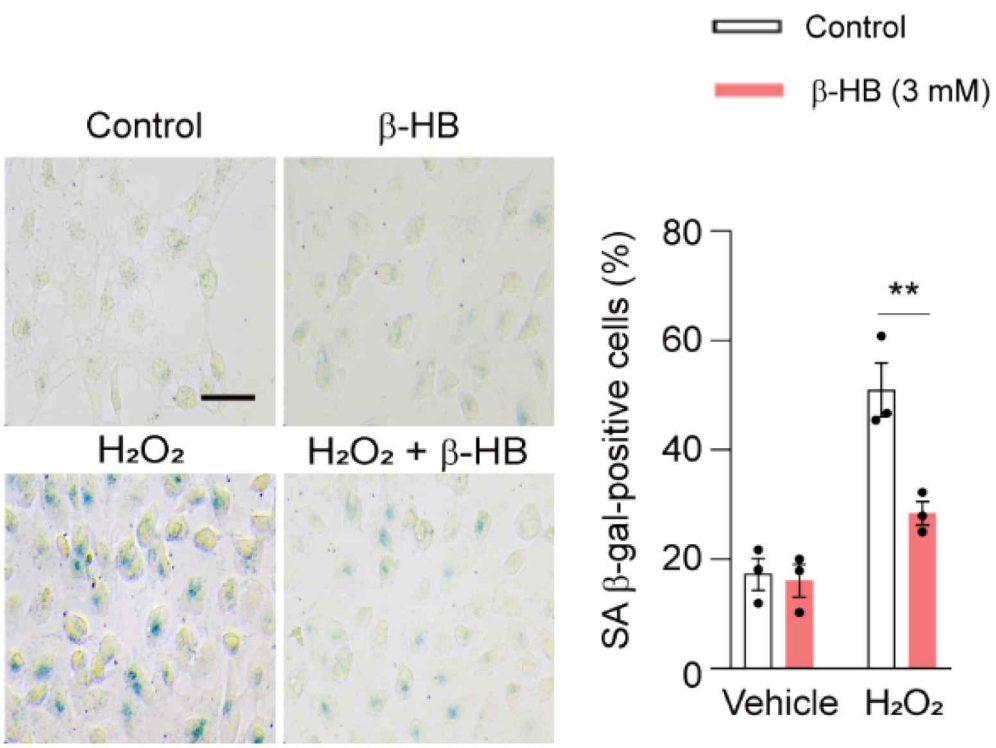

Figure 14. Representative images of SA β-gal staining in HK-2 cells

HK-2 cells were incubated with or without β-HB (3 mmol/L) for 24 h before H_2O_2 (500 μmol/L) stimulation for 6 h. Representative images of SA β-gal staining and quantification of SA β-gal-positive cells (n = 3 per group). **p < 0.01 vs H_2O_2 only. Scale bars=50 μm.

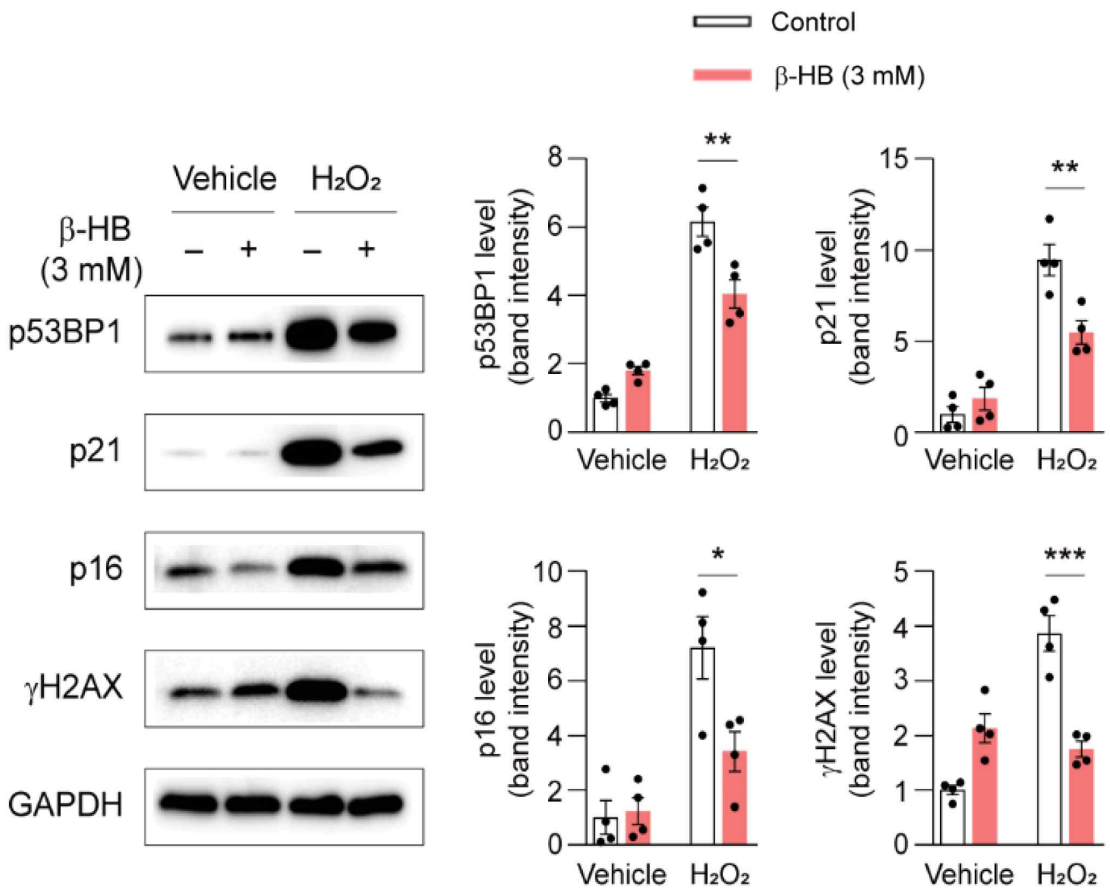

Figure 15. Western blot and band intensity for p21, p16, p53BP1, and γH2AX of HK-2 cells

HK-2 cells were incubated with or without β-HB (3 mmol/L) for 24 h before H_2O_2 (500 μmol/L) stimulation for 6 h. Relative protein expression of p21, p16, p53BP1, and γH2AX in the treated HK-2 cells (n = 4 per group). *p < 0.05, **p < 0.01, and ***p < 0.001 vs H_2O_2 only

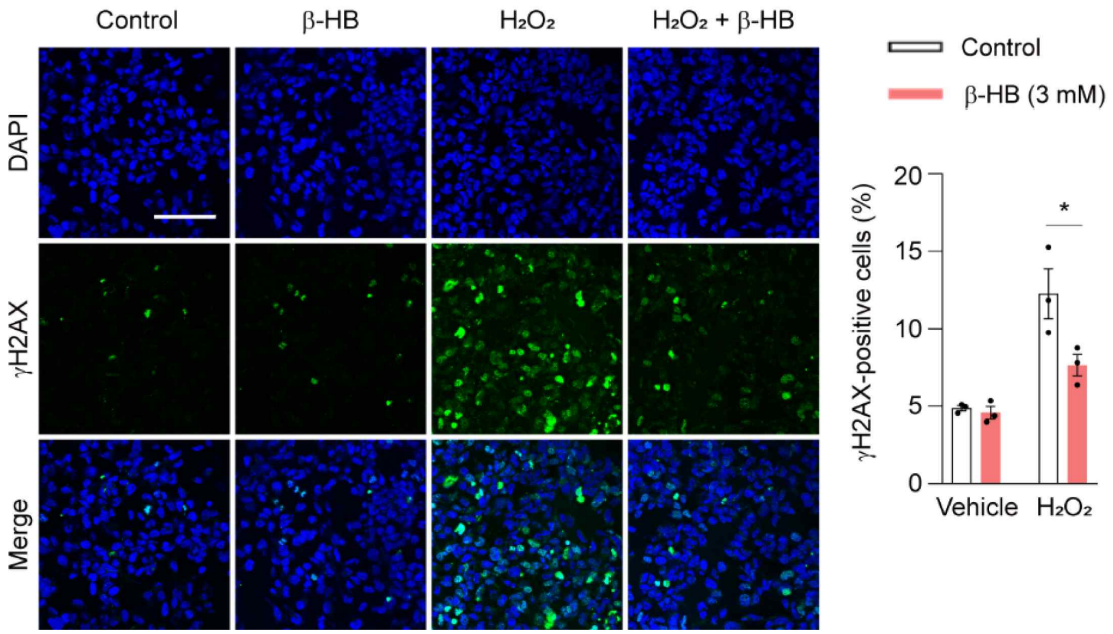

Figure 16. Immunofluorescence staining of γH2AX in HK-2 cells

HK-2 cells were incubated with or without β-HB (3 mmol/L) for 24 h before H_2O_2 (500 μmol/L) stimulation for 6 h. Immunofluorescence staining of γH2AX in the treated HK-2 cells (n = 3 per group). *p < 0.05 vs H_2O_2 only. Scale bars=50 μm.

β-Hydroxybutyrate attenuates H_2O_2-induced senescence in HK-2 cells

SGLT2 inhibitors are known to increase ketone body levels in the liver, kidney, and intestine [32]. Consistent with this, after 8 weeks of treatment, plasma β-HB concentrations were significantly higher in the *db/db*+SGLT2i group than in the other groups (Fig. 12). To investigate whether β-HB mediates the renoprotective effect of SGLT2 inhibitors, I pretreated the H_2O_2-induced senescent HK-2 cells with β-HB. After stimulation with H_2O_2, the expression levels of aging markers were increased compared with the control group. Interestingly, pretreatment with β-HB inhibited the increased mRNA expression of *p21*, *p16*, and *p53* (Fig. 13). Consistent with this, β-HB reduced the H_2O_2-induced senescence phenotypes, including SA β-gal, p53BP1, p21, p16, and γH2AX (Fig. 14, 15). The number of γH2AX-positive cells also increased with H_2O_2 but was inhibited by β-HB (Fig. 16). These data suggest that SGLT2 inhibitor-induced ketone bodies directly exert an anti-senescent effect to dampen cellular damage.

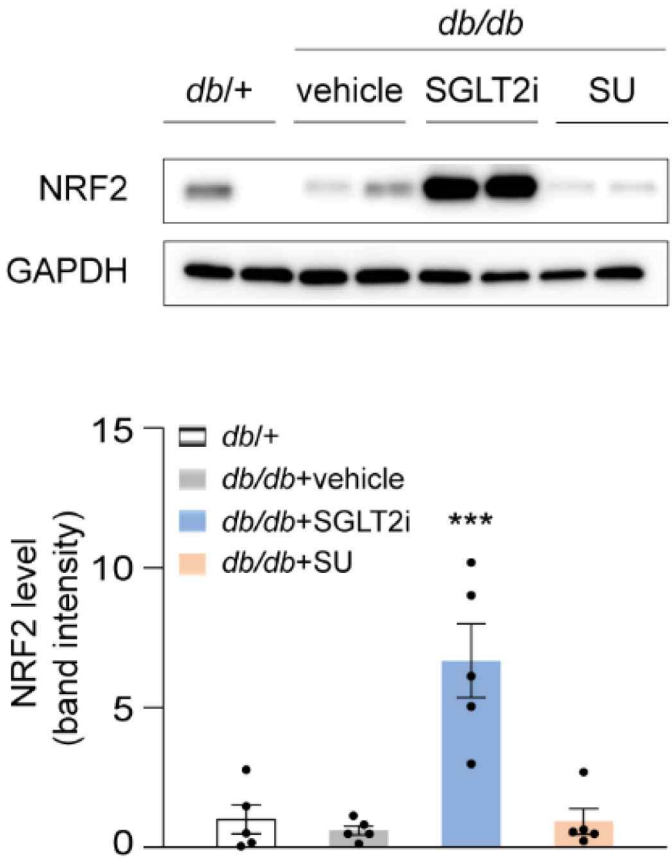

Figure 17. Western blot for NRF2 in the kidney

Western blot and band intensity for NRF2 in the kidney from the *db*/+, *db/db*+vehicle, *db/db*+SGLT2i, and *db/db*+SU mice (n = 5 per group). ***p < 0.001 vs *db/db*+vehicle

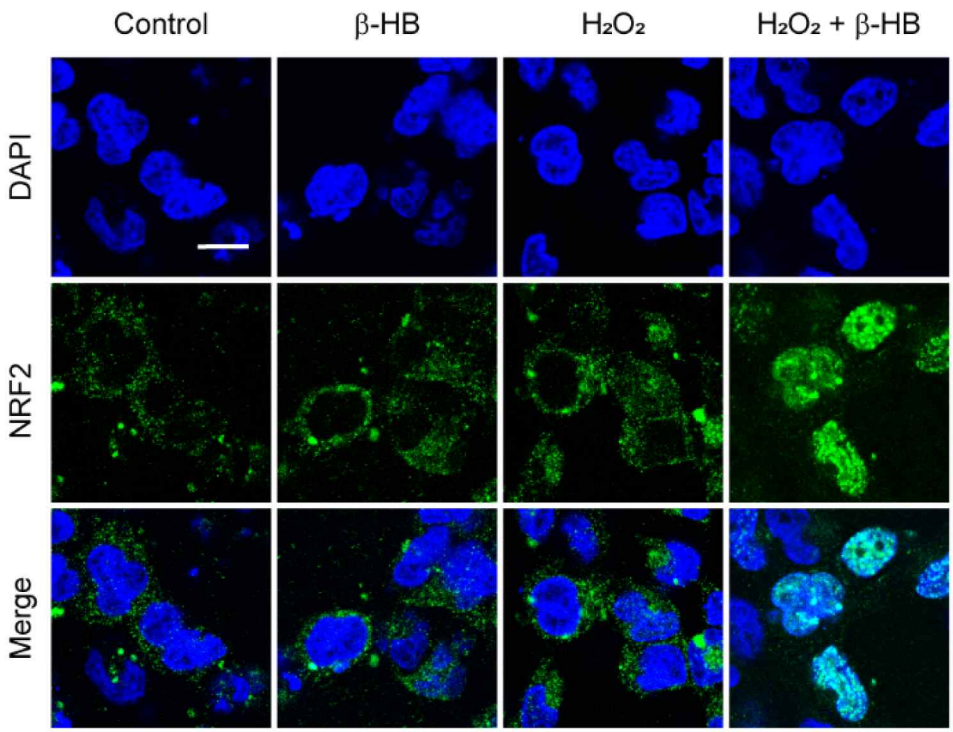

Figure 18. Immunofluorescence staining of NRF2 in HK-2 cells

HK-2 cells were incubated with or without β-HB (3 mmol/L) for 24 h before H_2O_2 (500 μmol/L) stimulation for 6 h. Representative images of immunofluorescence staining of NRF2 in the treated HK-2 cells. Scale bars=15 μm.

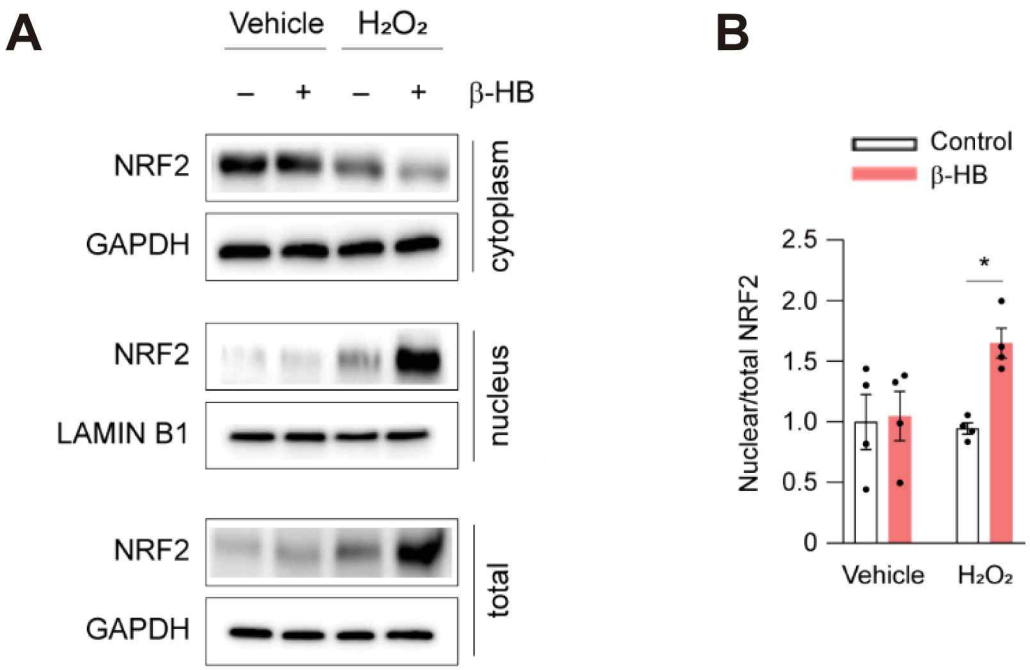

Figure 19. Protein levels of NRF2 in the cytoplasm, nucleus, and total lysates of HK-2 cells

HK-2 cells were incubated with or without β-HB (3 mmol/L) for 24 h before H_2O_2 (500 μmol/L) stimulation for 6 h. (A) Protein levels of NRF2 in the cytoplasm, nucleus, and total lysates of the treated HK-2 cells. The values of cytoplasm and nucleus were normalized against GAPDH and LAMIN B1 expression, respectively. (B) Nuclear NRF2 to total NRF2 ratio assessed via western blot (n = 4 per group). $^{**}p < 0.01$ vs H_2O_2 only

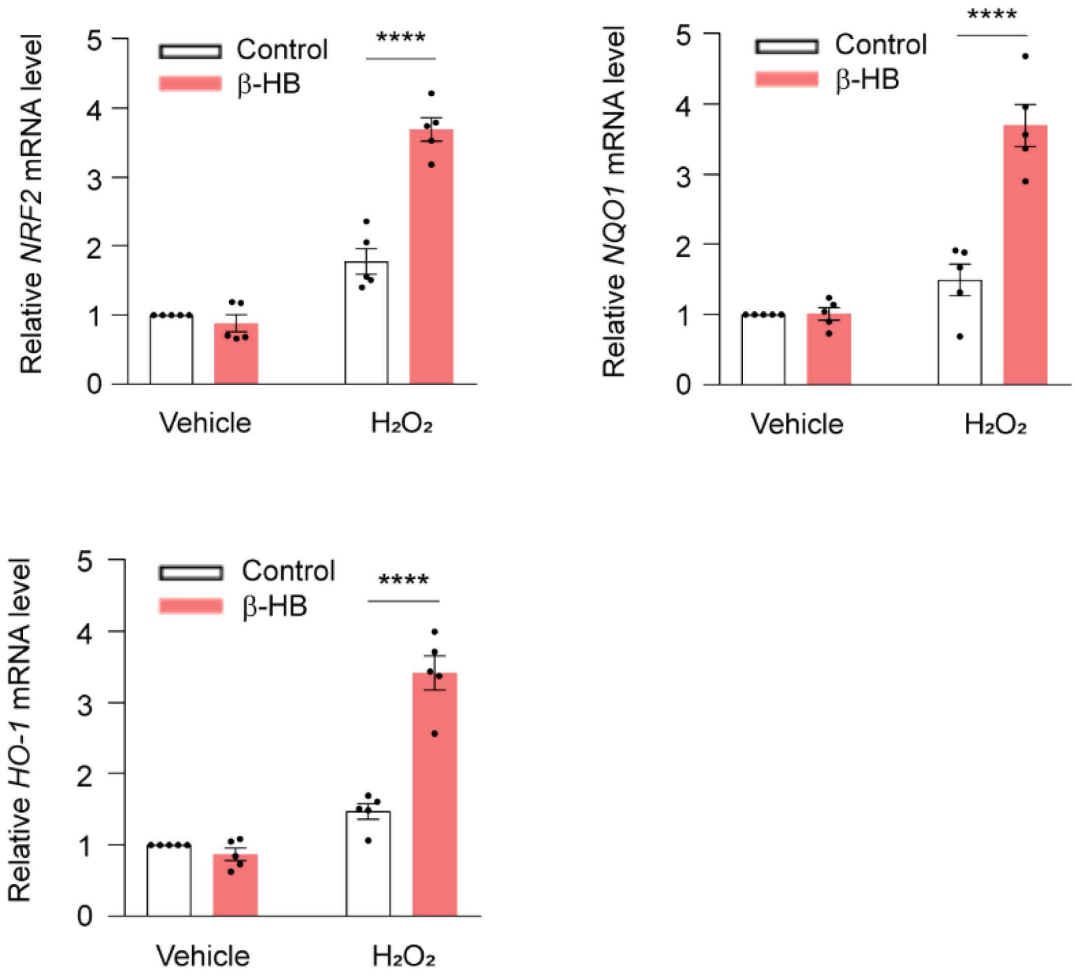

Figure 20. Relative mRNA expression of *NRF2*, *NQO1*, and *HO-1* in HK-2 cells

HK-2 cells were incubated with or without β-HB (3 mmol/L) for 24 h before H_2O_2 (500 μmol/L) stimulation for 6 h. Relative mRNA expression of *NRF2*, *NQO1*, and *HO-1* in the treated HK-2 cells (n = 5 per group). ****p < 0.0001 vs H_2O_2 only

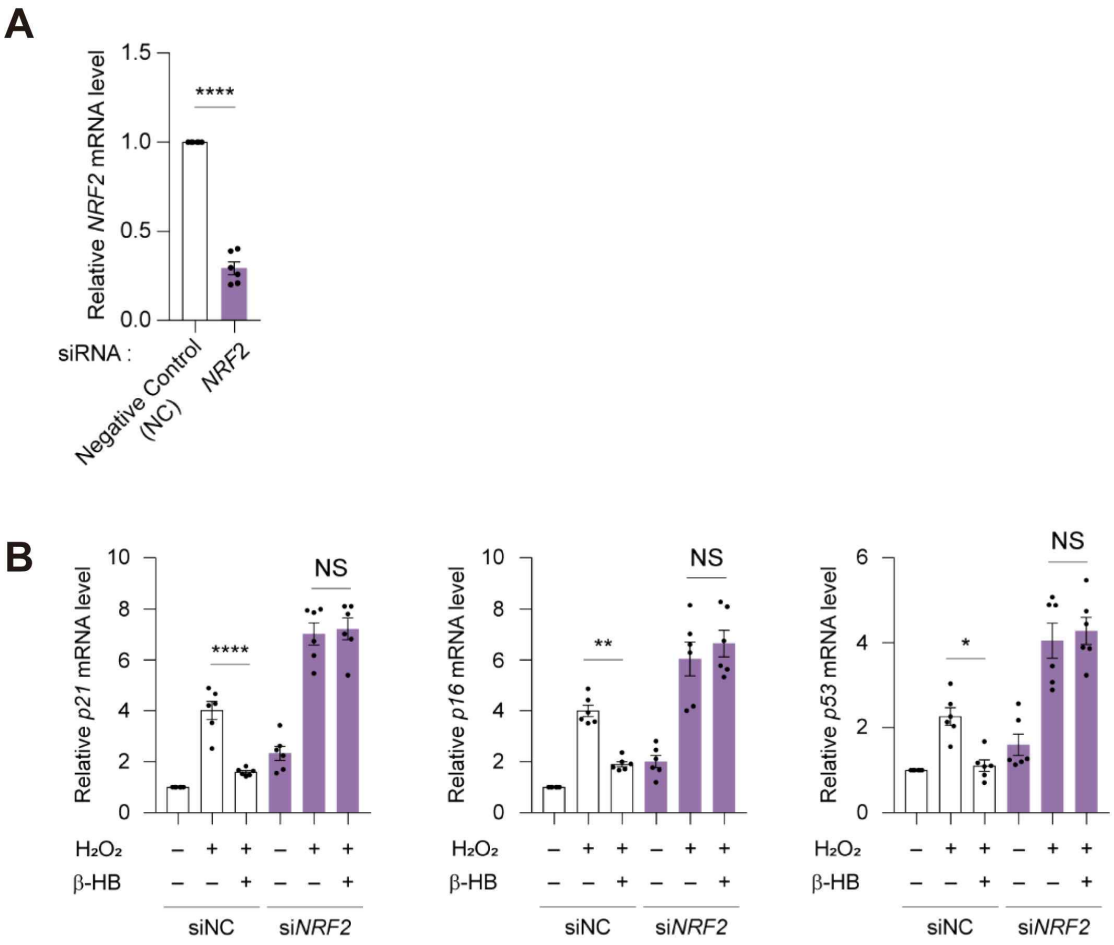

Figure 21. Relative mRNA expression of *NRF2* in siNC- or si*NRF2*-transfected HK-2 cells and relative mRNA expression of *p21*, *p16*, and *p53* with or without β-HB in siNC- or si*NRF2*-transfected HK-2 cells

(A) Relative mRNA expression of *NRF2* in siNC- or si*NRF2*-transfected HK-2 cells (n = 6 per group). (B) Relative mRNA expression of aging-related genes with or without β-HB in siNC- or si*NRF2*-transfected HK-2 cells (n = 6 per group). ****p < 0.0001 vs siNC (A). *p < 0.05, **p < 0.01, and ****p < 0.0001 vs H_2O_2 only (B). NC, negative control; NS, not significant

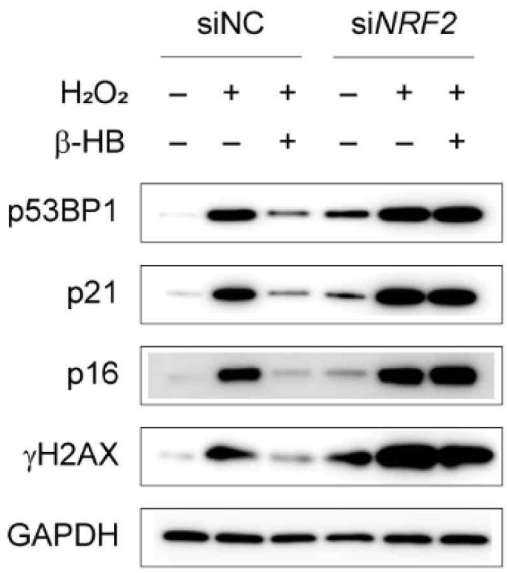

Figure 22. Protein expression of p21, p16, p53BP1, and γH2AX with or without β-HB in siNC- or si*NRF2*-transfected HK-2 cells

Relative protein expression of aging-related genes with or without β-HB in siNC- or si*NRF2*-transfected HK-2 cells.

β-Hydroxybutyrate induces NRF2 nuclear translocation in HK-2 cells

Ketone bodies are reported to induce NRF2 nuclear localization to activate the antioxidant pathway in the retina, hippocampus, and liver [33, 34]. Given that SGLT2 inhibitors reduce ROS levels in the diabetic kidney, I examined whether the NRF2 pathway was activated in this condition. Indeed, NRF2 protein levels were elevated in the kidney of the *db/db*+SGLT2i group but not in the *db/db*+SU group, compared with the *db/db*+vehicle group (Fig. 17). Besides, β-HB induced the translocation of NRF2 from the cytoplasm to the nucleus and the increase of nuclear NRF2 expression in the H_2O_2-induced senescent cells (Fig. 18, 19). The mRNA levels of *NRF2* downstream genes, including *NQO1* and *HO-1*, which have antioxidant properties, were markedly increased in the H_2O_2-induced senescent cells following treatment with β-HB (Fig. 20).

To investigate whether NRF2 is involved in the anti-senescent property, HK-2 cells were knocked down *NRF2* by siRNA transfection (Fig. 21A). The increase in the mRNA expression of *p21*, *p16*, and *p53* by H_2O_2 was significantly decreased by β-HB and siNC treatment. After *NRF2* knockdown by siRNA, the upregulation of the mRNA levels of *p21*, *p16*, and *p53* was more prominent under H_2O_2 treatment, but their expression levels were not inhibited by β-HB treatment (Fig. 21B). Likewise, the protein expression of p53BP1, p21, p16, and γH2AX exhibited a similar pattern (Fig. 22), suggesting that NRF2 mediates the anti-senescent effect of β-HB involved in the protection of DKD.

Discussion

Recent cardiovascular outcome trials including EMPA-REG OUTCOME, CANVAS, and DECLARE-TIMI 58 suggested that SGLT2 inhibitors (empagliflozin, canagliflozin, and dapagliflozin, respectively) might have renoprotective effects in patients with type 2 diabetes [7, 24, 25]. The risk of occurrence of renal outcomes, including sustained decrease in eGFR, new ESRD, or death from renal disease, was lower in these trials. In the CREDENCE study, a dedicated renal and cardiovascular outcome trial, type 2 diabetes patients with albuminuria (>300 mg/g) who were treated with either angiotensin-converting enzyme inhibitor or angiotensin receptor blocker were recruited. In that study, SGLT2 inhibition with canagliflozin decreased the risk of renal-specific composite end point as well as the risk of ESRD [26]. Furthermore, the DAPA-CKD study showed that dapagliflozin reduced the risk of worsening kidney function in patients with chronic kidney disease, regardless of the presence of type 2 diabetes [27]. Several mechanisms of kidney protection by SGLT2 inhibition have been suggested, including restoration of tubuloglomerular feedback and alleviation of renal hypoxia, which have been demonstrated in animal studies [5, 35], but there is still much to be revealed. Therefore, it is important to elucidate the mechanisms underlying the renoprotective effect of SGLT2 inhibitors.

In this study, I demonstrated that dapagliflozin prevents the progression of DKD by inhibiting cellular senescence in the kidney of a type 2 diabetes mouse model. The dapagliflozin-treated *db/db* mice exhibited lower expression levels of senescence markers, including *p21*, *p16*, and *p53*, in the kidney compared with *db/db* mice treated with glimepiride, a sulfonylurea. Oxidative stress and DNA damage were rescued in the glomerulus of *db/db* mice treated with dapagliflozin, but not with glimepiride. In H_2O_2-treated HK-2 cells, β-HB, which was increased in dapagliflozin-treated *db/db* mice, induced NRF2 nuclear translocation and activated downstream antioxidant pathways. In addition, dapagliflozin improved DKD phenotypes, including glomerular damage, mesangial expansion, and increased albumin excretion. Notably, these phenotypes were

independent of blood glucose levels, as they were not observed in the glimepiride-treated group.

In addition to chronological aging, metabolic stress accelerates cellular senescence in different target organs, which aggravates the control of metabolic disorders and leads to the development of complications, including DKD [15]. For instance, a high-fat/high-fructose diet increases the levels of oxidative stress and aging markers, including p16 and p53, in adipose tissues, which in turn increases proinflammatory cytokine production and aggravates insulin resistance [36, 37]. Hypertension promotes cellular senescence in the human kidney by inducing p16 expression via activation of the p38 mitogen-activated protein kinase pathway [38]. Similarly, hyperglycemic stress has been reported to accelerate renal senescence through the loss of regenerative capacity via the p16-pRB-senescence pathway and telomere shortening [14]. These studies suggest that maintenance of metabolic homeostasis is necessary to mitigate cellular senescence and prevent complications. However, as glimepiride treatment did not show any beneficial effects on cellular senescence in the kidney of *db/db* mice, the anti-senescent effect of dapagliflozin could not be explained by its alleviation of hyperglycemia alone.

The anti-senescent effect of SGLT2 inhibitors on DKD has not been fully elucidated. In this study, I found some clues connecting SGLT2 inhibition-induced ketogenesis and NRF2-mediated enhancement of the antioxidant system. SGLT2 inhibitors are well known to increase the plasma levels of ketone bodies [39, 40]. Ketone bodies have been shown to activate antioxidant pathways by inducing the expression of NRF2 in the retina, hippocampus, and liver [33, 34]. Several mediators, including fumarate, histone deacetylase inhibitor, and lipid peroxide, have been reported to mediate the ketone body-induced NRF2 expression [33, 34, 41-43]. NRF2 is involved in the transcription of antioxidant genes, including *NQO1* and *HO-1* [41, 44], thereby mitigating oxidative stress and cellular senescence [45-47]. Consistently, plasma β-HB levels were markedly increased in the *db/db*+SGLT2i group, and β-HB induced the translocation of NRF2 into the nucleus of the H_2O_2-treated HK-2 cells, which mitigated oxidative stress and cellular senescence. Future studies should evaluate the possible

contribution of anti-senescent properties of SGLT2 inhibitors on metabolic phenotypes in other tissues.

SASP factors are secreted in response to cellular stress, including DNA damage and oxidative stress [48, 49], which in turn induce insulin resistance, endoplasmic reticulum stress, and chronic inflammation [50, 51]. Senolytics eliminate senescent cells, thereby reducing SASP factors to protect adjacent cells from further deterioration [52]. In the current study, SASP factors, including MIP-1γ, MIP-2, and CXCL-related cytokines in the kidney, were significantly reduced by dapagliflozin. This suggests that SGLT2 inhibitors can be considered as senomorphics modulating SASP factors [53]. SGLT2 inhibition reduces inflammation in the kidney [5, 54], but the underlying mechanism is yet to be elucidated. The anti-senescent effect of SGLT2 inhibition may be a potential mechanism explaining the anti-inflammatory effect of SGLT2 inhibitors by decreasing SASP.

This study presents several metabolic implications for SGLT2 inhibitors. The dapagliflozin-treated group showed improved beta cell function in *db/db* mice compared with the vehicle-treated control group. It was reported that dapagliflozin improved beta cell sensitivity to glucose as well as to incretin hormones in patients with type 2 diabetes [55], where reduced glucotoxicity could be a suggested mechanism [56]. Moreover, dapagliflozin treatment increased the food intake in *db/db* mice, which already exhibited severe hyperphagia at baseline. An Adaptive increase in energy intake against energy loss via glycosuria has been predicted in a mathematical model based on the data of 86 patients with type 2 diabetes taking empagliflozin for 90 weeks [57]. The mechanisms underlying increased energy intake after SGLT2 inhibition need to be further investigated.

This study has some limitations. First, in this study, no senescent cells were observed in kidney components other than the glomerulus. In the diabetic kidneys, the expressions of γH2AX were found only in the glomerulus, but not in the tubule. In contrast, the levels of DHE-fluorescence were found in both glomerulus and tubule. These results may be explained by attenuating glomerular hyperfiltration with dapagliflozin treatment, although dapagliflozin mainly acts in the proximal tubule.

However, there might have been sequential changes in the level of oxidative stress starting from the tubule and then migrating to the glomerulus. Sequential analysis at different time points would be necessary. Second, the results of cytokine array were demonstrated in whole kidney tissues, not the isolated glomerulus. Third, this study was not performed animal experiments to validate the role of ketone body-induced NRF2 in the diabetic kidney. Further studies using *NRF2* knockout or overexpression animal models should be performed.

In conclusion, dapagliflozin, an SGLT2 inhibitor, reduced cellular senescence in the kidney of a type 2 diabetes mouse model, independent of its glucose-lowering effect. β-HB mediated the anti-senescent effect of dapagliflozin by stimulating the NRF2 nuclear translocation and activating the antioxidant pathway. These results provide a basis for further research into the development of new therapeutic strategies targeting senescence in the treatment and prevention of diabetic complications, including DKD.

Acknowledgements

I thank Professor Kyung Chul Moon for helping me with the interpretation of renal histology data and Doctor Joon Ho Moon for helpful comments on clinical implication.

References

1. Reutens, A.T., Epidemiology of diabetic kidney disease. Med Clin North Am, 2013. 97(1): p. 1-18.
2. Tervaert, T.W., et al., Pathologic classification of diabetic nephropathy. J Am Soc Nephrol, 2010. 21(4): p. 556-63.
3. Cooper, M.E., Interaction of metabolic and haemodynamic factors in mediating experimental diabetic nephropathy. Diabetologia, 2001. 44(11): p. 1957-72.
4. Vallon, V., The proximal tubule in the pathophysiology of the diabetic kidney. Am J Physiol Regul Integr Comp Physiol, 2011. 300(5): p. R1009-22.
5. Heerspink, H.J.L., et al., Renoprotective effects of sodium-glucose cotransporter-2 inhibitors. Kidney Int, 2018. 94(1): p. 26-39.
6. Muskiet, M.H.A., D.C. Wheeler, and H.J.L. Heerspink, New pharmacological strategies for protecting kidney function in type 2 diabetes. Lancet Diabetes Endocrinol, 2019. 7(5): p. 397-412.
7. Wiviott, S.D., et al., Dapagliflozin and Cardiovascular Outcomes in Type 2 Diabetes. N Engl J Med, 2019. 380(4): p. 347-357.
8. Zinman, B., et al., Empagliflozin, Cardiovascular Outcomes, and Mortality in Type 2 Diabetes. N Engl J Med, 2015. 373(22): p. 2117-28.
9. Nangaku, M., Chronic hypoxia and tubulointerstitial injury: a final common pathway to end-stage renal failure. J Am Soc Nephrol, 2006. 17(1): p. 17-25.
10. Hansell, P., et al., Determinants of kidney oxygen consumption and their relationship to tissue oxygen tension in diabetes and hypertension. Clin Exp Pharmacol Physiol, 2013. 40(2): p. 123-37.
11. Haase, V.H., Mechanisms of hypoxia responses in renal tissue. J Am Soc Nephrol, 2013. 24(4): p. 537-41.
12. Chang, Y.K., et al., Dapagliflozin, SGLT2 Inhibitor, Attenuates Renal Ischemia-Reperfusion Injury. PLoS One, 2016. 11(7): p. e0158810.
13. Packer, M., Mechanisms Leading to Differential Hypoxia-Inducible Factor

Signaling in the Diabetic Kidney: Modulation by SGLT2 Inhibitors and Hypoxia Mimetics. Am J Kidney Dis, 2020.

14. Verzola, D., et al., Accelerated senescence in the kidneys of patients with type 2 diabetic nephropathy. Am J Physiol Renal Physiol, 2008. 295(5): p. F1563-73.
15. Khosla, S., et al., The role of cellular senescence in ageing and endocrine disease. Nat Rev Endocrinol, 2020. 16(5): p. 263-275.
16. DeFronzo, R.A., L. Norton, and M. Abdul-Ghani, Renal, metabolic and cardiovascular considerations of SGLT2 inhibition. Nat Rev Nephrol, 2017. 13(1): p. 11-26.
17. Nourbakhsh, N. and P. Singh, Role of renal oxygenation and mitochondrial function in the pathophysiology of acute kidney injury. Nephron Clin Pract, 2014. 127(1-4): p. 149-52.
18. Bartlett, D.E., et al., The Role of Na/K-ATPase Signaling in Oxidative Stress Related to Aging: Implications in Obesity and Cardiovascular Disease. Int J Mol Sci, 2018. 19(7).
19. Shintani, H., et al., Calorie Restriction Mimetics: Upstream-Type Compounds for Modulating Glucose Metabolism. Nutrients, 2018. 10(12).
20. Miller, R.A., et al., Canagliflozin extends lifespan in genetically heterogeneous male but not female mice. JCI Insight, 2020.
21. Sohal, R.S. and M.J. Forster, Caloric restriction and the aging process: a critique. Free Radic Biol Med, 2014. 73: p. 366-82.
22. Mattison, J.A., et al., Caloric restriction improves health and survival of rhesus monkeys. Nat Commun, 2017. 8: p. 14063.
23. Puchalska, P. and P.A. Crawford, Multi-dimensional Roles of Ketone Bodies in Fuel Metabolism, Signaling, and Therapeutics. Cell Metab, 2017. 25(2): p. 262-284.
24. Neal, B., et al., Canagliflozin and Cardiovascular and Renal Events in Type 2 Diabetes. N Engl J Med, 2017. 377(7): p. 644-657.
25. Wanner, C., et al., Empagliflozin and Progression of Kidney Disease in Type 2 Diabetes. N Engl J Med, 2016. 375(4): p. 323-34.

26. Perkovic, V., et al., Canagliflozin and Renal Outcomes in Type 2 Diabetes and Nephropathy. N Engl J Med, 2019. 380(24): p. 2295-2306.
27. Heerspink, H.J.L., et al., Dapagliflozin in Patients with Chronic Kidney Disease. N Engl J Med, 2020. 383(15): p. 1436-1446.
28. Sharma, K., P. McCue, and S.R. Dunn, Diabetic kidney disease in the db/db mouse. Am J Physiol Renal Physiol, 2003. 284(6): p. F1138-44.
29. Pole, A., M. Dimri, and G.P. Dimri, Oxidative stress, cellular senescence and ageing. Aims Molecular Science, 2016. 3(3): p. 300-324.
30. Pansarasa, O., et al., Age-dependent changes of antioxidant activities and markers of free radical damage in human skeletal muscle. Free Radic Biol Med, 1999. 27(5-6): p. 617-22.
31. Aydin, A.F., et al., The effect of carnosine treatment on prooxidant-antioxidant balance in liver, heart and brain tissues of male aged rats. Biogerontology, 2010. 11(1): p. 103-9.
32. Kim, J.H., et al., Sodium-glucose cotransporter 2 inhibitors regulate ketone body metabolism via inter-organ crosstalk. Diabetes Obes Metab, 2019. 21(4): p. 801-811.
33. Izuta, Y., et al., Ketone body 3-hydroxybutyrate mimics calorie restriction via the Nrf2 activator, fumarate, in the retina. Aging Cell, 2018. 17(1).
34. Milder, J.B., L.P. Liang, and M. Patel, Acute oxidative stress and systemic Nrf2 activation by the ketogenic diet. Neurobiol Dis, 2010. 40(1): p. 238-44.
35. Hesp, A.C., et al., The role of renal hypoxia in the pathogenesis of diabetic kidney disease: a promising target for newer renoprotective agents including SGLT2 inhibitors? Kidney Int, 2020. 98(3): p. 579-589.
36. Minamino, T., et al., A crucial role for adipose tissue p53 in the regulation of insulin resistance. Nat Med, 2009. 15(9): p. 1082-7.
37. Schafer, M.J., et al., Exercise Prevents Diet-Induced Cellular Senescence in Adipose Tissue. Diabetes, 2016. 65(6): p. 1606-15.
38. Westhoff, J.H., et al., Hypertension induces somatic cellular senescence in rats and humans by induction of cell cycle inhibitor p16INK4a. Hypertension, 2008.

52(1): p. 123-9.

39. Verma, S., et al., Empagliflozin Increases Cardiac Energy Production in Diabetes: Novel Translational Insights Into the Heart Failure Benefits of SGLT2 Inhibitors. JACC Basic Transl Sci, 2018. 3(5): p. 575-587.

40. Kim, S.R., et al., SGLT2 inhibition modulates NLRP3 inflammasome activity via ketones and insulin in diabetes with cardiovascular disease. Nat Commun, 2020. 11(1): p. 2127.

41. Rojas-Morales, P., J. Pedraza-Chaverri, and E. Tapia, Ketone bodies, stress response, and redox homeostasis. Redox Biol, 2020. 29: p. 101395.

42. Shimazu, T., et al., Suppression of oxidative stress by beta-hydroxybutyrate, an endogenous histone deacetylase inhibitor. Science, 2013. 339(6116): p. 211-4.

43. Wang, B., et al., Histone deacetylase inhibition activates transcription factor Nrf2 and protects against cerebral ischemic damage. Free Radic Biol Med, 2012. 52(5): p. 928-36.

44. Tonelli, C., I.I.C. Chio, and D.A. Tuveson, Transcriptional Regulation by Nrf2. Antioxid Redox Signal, 2018. 29(17): p. 1727-1745.

45. Yin, Z.W., et al., The transcription factor Nrf2 might be involved in the process of renal aging. International Journal of Clinical and Experimental Medicine, 2019. 12(5): p. 5405-5411.

46. Fulop, G.A., et al., Nrf2 deficiency in aged mice exacerbates cellular senescence promoting cerebrovascular inflammation. Geroscience, 2018. 40(5-6): p. 513-521.

47. Schmidlin, C.J., et al., Redox regulation by NRF2 in aging and disease. Free Radic Biol Med, 2019. 134: p. 702-707.

48. Kang, C., et al., The DNA damage response induces inflammation and senescence by inhibiting autophagy of GATA4. Science, 2015. 349(6255): p. aaa5612.

49. Hernandez-Segura, A., J. Nehme, and M. Demaria, Hallmarks of Cellular Senescence. Trends Cell Biol, 2018. 28(6): p. 436-453.

50. Palmer, A.K., et al., Cellular senescence: at the nexus between ageing and diabetes. Diabetologia, 2019. 62(10): p. 1835-1841.

51. Soto-Gamez, A., W.J. Quax, and M. Demaria, Regulation of Survival Networks in Senescent Cells: From Mechanisms to Interventions. J Mol Biol, 2019. 431(15): p. 2629-2643.
52. van Deursen, J.M., Senolytic therapies for healthy longevity. Science, 2019. 364(6441): p. 636-637.
53. von Kobbe, C., Targeting senescent cells: approaches, opportunities, challenges. Aging (Albany NY), 2019. 11(24): p. 12844-12861.
54. Heerspink, H.J.L., et al., Canagliflozin reduces inflammation and fibrosis biomarkers: a potential mechanism of action for beneficial effects of SGLT2 inhibitors in diabetic kidney disease. Diabetologia, 2019. 62(7): p. 1154-1166.
55. Ahn, C.H., et al., Sodium-glucose cotransporter-2 inhibition improves incretin sensitivity of pancreatic beta-cells in people with type 2 diabetes. Diabetes Obes Metab, 2018. 20(2): p. 370-377.
56. Merovci, A., et al., Dapagliflozin lowers plasma glucose concentration and improves β-cell function. J Clin Endocrinol Metab, 2015. 100(5): p. 1927-32.
57. Ferrannini, G., et al., Energy Balance After Sodium-Glucose Cotransporter 2 Inhibition. Diabetes Care, 2015. 38(9): p. 1730-5.

논 문 초 록

2형 당뇨병 동물 모델에서 SGLT2 억제제의 신장 세포 노화 억제 효과

서론

Sodium-glucose cotransporter 2 (SGLT2) 억제제는 당뇨병성 신증의 진행을 억제한다고 알려져 있다. 그러나 그 기전에 대해서는 아직 완전히 밝혀져 있지 않다. 본 연구에서는 SGLT2 억제제가 신장 세포의 노화를 억제하는 지 알아보고, 그 분자적 기전을 밝히고자 한다.

방법

Dapagliflozin (1 mg/kg/day), glimepiride (2.5 mg/kg/day), 또는 vehicle을 *db/db* 생쥐에 8 주간 경구로 투약했다. *db/db* 생쥐의 신장 세포 노화는 p21, p16, p53, γH2AX 유전자를 real-time RT-PCR, 면역염색, 웨스턴 블롯 등의 방법으로 측정하였다. 또한, *in vitro*에서 HK-2 신장 세포를 H_2O_2로 전처리하여 세포 노화를 유도하고, β-hydroxybutyrate (β-HB) 또는 si*NRF2*를 처리하여 노화 관련 표현형을 조사하였다.

결과

Dapagliflozin은 *db/db* 생쥐의 신장에서 메산지움 확장을 억제하였고, 사구체의 크기를 줄였으며, 알부민 배설을 감소시켰다. 노화 마커인 p21, p16, p53, γH2AX 유전자의 신장 내 발현 수준은 *db*/+ 그룹과 비교하여, *db/db*+vehicle 그룹에서 증가하였고, 이 증가는 *db/db*+SGLT2i 그룹에서 감소하였지만, *db/db*+SU 그룹에서는 감소하지 않았다. 또한, *db/db*+SGLT2i 그룹의 산화 스트레스 수준은 *db/db*+vehicle, *db/db*+SU 그

룹과 비교하여 유의하게 감소하였다. Dapagliflozin은 혈장 β-HB 농도를 증가시켰고, β-HB는 HK-2 세포에서 H_2O_2로 유도된 DNA 손상 및 노화 현상을 감소시켰다. 또한, β-HB 처리는 NRF2를 핵 내로 이동시켰고, 이는 항산화 경로를 활성화하여 항노화 효과를 매개하였다.

결론

SGLT2 억제제인 dapagliflozin은 혈중 케톤 농도 증가를 통해 신장 세포의 NRF2 활성화를 매개하여 산화 스트레스를 억제함으로써 신장 세포의 노화를 방지하고, 이에 따라 당뇨병성 신증의 진행을 억제하였다.

주요어 : SGLT2 억제제, 세포 노화, 당뇨병성 신증, 케톤체, NRF2
학 번 : 2019-27807